HHS Public Access

Author manuscript

Cancer Res. Author manuscript; available in PMC 2022 March 15.

Published in final edited form as:

Cancer Res. 2021 September 15; 81(18): 4736–4750. doi:10.1158/0008-5472.CAN-21-0307.

RNA splicing factors SRRM3 and SRRM4 distinguish molecular phenotypes of castration-resistant neuroendocrine prostate cancer

Mark P. Labrecque[1], **Lisha G. Brown**[1], **Ilsa M. Coleman**[2,3], **Bryce Lakely**[1], **Nicholas J. Brady**[4], **John K. Lee**[2,3], **Holly M. Nguyen**[1], **Dapei Li**[5], **Brian Hanratty**[2], **Michael C. Haffner**[2,3,6], **David S. Rickman**[4], **Lawrence D. True**[1,6], **Daniel W. Lin**[1,7], **Hung-Ming Lam**[1], **Joshi J. Alumkal**[8], **Eva Corey**[1], **Peter S. Nelson**[2,3,5,*], **Colm Morrissey**[1,*]

[1]Department of Urology, University of Washington, Seattle, WA

[2]Divison of Human Biology, Fred Hutchinson Cancer Research Center, Seattle, WA

[3]Divison of Clinical Research, Fred Hutchinson Cancer Research Center, Seattle, WA

[4]Department of Pathology and Laboratory Medicine, Weill Cornell Medicine, New York, NY

[5]Department of Medicine, Division of Medical Oncology, University of Washington, Seattle, WA

[6]Department of Laboratory Medicine and Pathology, University of Washington, Seattle, WA

[7]Division of Public Health Sciences, Fred Hutchinson Cancer Research Center, Seattle, WA

[8]Department of Internal Medicine, Rogel Cancer Center, University of Michigan, Ann Arbor, MI

Abstract

Neuroendocrine (NE) differentiation in metastatic castration-resistant prostate cancer (mCRPC) is an increasingly common clinical feature arising from cellular plasticity. We recently characterized two mCRPC phenotypes with NE features: androgen receptor (AR)-positive NE-positive amphicrine prostate cancer (AMPC) and AR-negative small cell or neuroendocrine prostate cancer (SCNPC). Here, we interrogated the regulation of RE1-silencing transcription factor (REST), a transcriptional repressor of neuronal genes, and elucidated molecular programs driving AMPC and SCNPC biology. Analysis of prostate cancer (PC) cell lines, mCRPC specimens, and LuCaP patient-derived xenograft models detected alternative splicing of REST to REST4 and attenuated REST repressor activity in AMPC and SCNPC. The REST locus was also hypermethylated and REST expression was reduced in SCNPC. While serine/arginine repetitive matrix protein 4

[*]Corresponding authors: Colm Morrissey PhD, Genitourinary Cancer Research Laboratory, Department of Urology, Box 356510, University of Washington, Seattle, WA 98195, cmorriss@uw.edu, Peter S. Nelson MD, Divisions of Human Biology and Clinical Research, Fred Hutchinson Cancer Research Center, Mailstop D4-100, 1100 Eastlake, Seattle, WA 98109-1024, pnelson@fhcrc.org.

AUTHOR CONTRIBUTIONS

MPL, PSN and CM conceived and designed the project. MPL, IMC, NJB, DJR, DL, BH, MCH and HML performed sequencing and bioinformatics analyses. MPL, LGB, BL, and JKL conducted molecular and cell biology experiments. LDT provided pathology expertise. HMN, EC, and CM provided biospecimens and patient-derived xenograft models. DWL, JJA and PSN provided clinical and technical expertise. MPL wrote the manuscript and all authors reviewed and edited the manuscript.

Conflict of interest statements: Conflict of interest statements: DSR reports research funding from Janssen Pharmaceuticals, outside of the submitted work. LDT reports equity ownership of Lightspeed Microscopy, Inc, outside of the submitted work. PSN reports income received for advisory work for Janssen, Bristol Myers Squibb and Merck and expert testimony from Venable-Fitzpatrick LLP, outside of the submitted work.

(SRRM4) was previously implicated in alternative splicing of REST in mCRPC, we detected SRRM3 expression in REST4-positive, SRRM4-negative AMPC and SCNPC. In CRPC cell lines, SRRM3 induced alternative splicing of REST to REST4 and exacerbated the expression of REST-repressed genes. Furthermore, SRRM3 and SRRM4 expression defined molecular subsets of AMPC and SCNPC across species and tumor types. Two AMPC phenotypes and three SCNPC phenotypes were characterized, denoted either by REST attenuation and ASCL1 activity or by progressive activation of neuronal transcription factor programs, respectively. These results nominate SRRM3 as the principal REST splicing factor expressed in early NE differentiation and provide a framework to molecularly classify diverse NE phenotypes in mCRPC.

INTRODUCTION

Prostate cancer (PC) cell growth and survival typically relies on androgen receptor (AR) activity, therefore, therapeutic interventions targeting the AR signaling axis are cornerstones for PC therapy. However, sustained AR pathway inhibition induces selective pressures on heterogeneous tumors containing cell populations with intrinsic resistance mechanisms or plastic natures. Thus, treatment-resistant metastatic castration-resistant prostate cancer (mCRPC) arises through diverse bypass mechanisms to subvert AR-directed therapies, including AR amplification, mutation or expression of AR splice variants (1–3); adoption of alternative nuclear receptors to sustain cell growth (4); and transdifferentiation to AR-null phenotypes (5–7).

Small cell or neuroendocrine prostate cancer (SCNPC) comprises a spectrum of clinical disease states that include *de novo* primary SCNPC to treatment-emergent metastatic SCNPC (8). While *de novo* SCNPC is rare, the incidence of treatment-emergent SCNPC is rising (5,9,10). In addition, metastatic SCNPC is typically AR-null and histologically defined by small, round tumor cells that express neuroendocrine (NE) biomarkers synaptophysin (SYP), chromogranin A (CHGA) and/or CD56/NCAM1 (8). However, the observation of novel treatment-resistant subtypes and the diverse molecular mechanisms contributing to lineage plasticity and NE transdifferentiation have led to a more complex and incomplete understanding of SCNPC biology. For example, loss of key tumor suppressors such as *TP53* and *RB1* (11); upregulation of pioneer and neural transcription factors such as MYCN (12), POU3F2 (13) and SOX2 (14); and epigenomic alterations associated with EZH2 (15) have all been implicated in facilitating lineage switching. However, SCNPC is not an obligate endpoint for CRPC tumor cells with *TP53* and *RB1* loss (16), and clinical studies have described subsets of SCNPC with retained AR expression and activity (17). In addition, the temporal and spatial interplay of identified transcription factor programs are not well understood in SCNPC and their relevance in the context of varying genomic backgrounds to cellular plasticity remains an active area of investigation.

Transcriptome profiling has facilitated the classification of cancers into subtypes with distinct functional features. We previously employed whole-transcriptome RNA sequencing (RNAseq) and immunohistochemical studies across mCRPC biospecimens and LuCaP patient-derived xenograft (PDX) models and identified five mCRPC molecular phenotypes; (i) AR-high PC (ARPC); (ii) AR-low PC (ARLPC); (iii) amphicrine PC (AMPC) composed

of tumor cells co-expressing AR and NE programs (AR^+/NE^+); (iv) double-negative PC (DNPC) that lacks AR and NE gene expression (AR^-/NE^-); and (v) SCNPC (AR^-/NE^+; Ref. (7)).

Our group and others have highlighted the central role of AR and RE1-silencing transcription factor (REST) programs in defining CRPC molecular phenotypes (7,18–21). REST is a master regulator of differentiation that represses neuronal programs in non-neuronal cells. Alternative splicing of *REST* transcripts by serine/arginine repetitive matrix protein 4 (SRRM4) has been implicated in the loss of REST repressor activity in neurogenesis and NE^+ tumors (21–23). SRRM4 incorporates exon N3c into the *REST* transcript, leading to the expression of a truncated REST protein (REST4) that lacks the C-terminus transcriptional repressor domain, and induction of neuronal gene expression (23,24). However, the molecular underpinnings of REST regulation in clinical mCRPC specimens and the biological impacts of attenuated REST activity as it relates to novel mCRPC phenotypes are not fully understood. The work we describe herein was designed to address these deficits.

MATERIALS AND METHODS

Tissue acquisition:

The Institutional Review Board of the University of Washington approved this study (protocol no. 2341). All rapid autopsy tissues were collected from patients who signed written informed consent under the aegis of the Prostate Cancer Donor Program at the University of Washington (25). Biospecimens were obtained within 8 hours of death from patients who died of metastatic CRPC as previously described (7,26). All patient-derived xenograft experiments were approved by the University of Washington Institutional Animal Care and Use Committee (protocol no. 3202–01). LuCaP patient-derived xenograft (PDX) lines were established from specimens acquired at either radical prostatectomy or at autopsy, implanted, and maintained by serial passage in immune compromised male mice as previously described (27). All mice used for the human MYCN-expressing mouse model were maintained and all procedures were performed following protocols approved by the Weill Cornell Medicine Institutional Animal Care and Use Committee (protocol no. 2008-0019).

Cell lines:

All cells were maintained at 37°C in humidified Steri-Cult CO_2 incubators (Thermo Scientific). C4–2B cells (gift from L. Chung, Cedars-Sinai Medical Center, Los Angeles, CA), DU145 cells (ATCC) and 22Rv1 cells (gift from S. Plymate University of Washington) were maintained in RPMI-1640 Media (Gibco, Life Technologies) with 10% fetal bovine serum (Atlanta Biologicals). VCaP cells (purchased directly from ATCC; CRL-2876) were maintained in DMEM (ATCC) with 10% fetal bovine serum (Atlanta Biologicals). NCI-H660 (purchased directly from ATCC; CRL-5813) cells were maintained in HITES media (ATCC) supplemented with 5% FBS. All cell lines used in this project were validated through STR analysis using ATCC reference genomes and were routinely tested for mycoplasma using the MycoFluor Mycoplasma Detection Kit (Invitrogen).

PCR and sequencing:

First-strand cDNA synthesis was performed with 1 μg of RNA using an Advantage RT-for-PCR Kit (Clontech Laboratories). PCR was performed using either Platinum SYBR Green qPCR SuperMix-UDG (Invitrogen; qPCR and Screening PCR) or HotStarTaq Plus Master Mix (Qiagen; Sequencing PCR) on a Rotor-Gene Q (Qiagen). All primer set sequences are listed in Supplementary Table S1. Touchdown PCR was used for both screening and sequencing PCR followed by agarose gel electrophoresis (Supplementary Materials and Methods).

Transient transfections and lentiviral transductions:

For ectopic expression studies, cells were transfected with Tru ORF Gold expression vectors (OriGene) for SRRM3 (CAT#: RC226066), SRRM4 (CAT#: SC314194), pCMV6-Entry (CAT#: ps100001) or pCMV6-Neo (CAT#: PCMV6NEO) using the TransIT-X2 Transfection Reagent (Mirus Bio) according to manufacturer's protocols. For siRNA knockdown studies, 22Rv1 cells were transfected with ON-TARGETplus pooled siRNA (Horizon Discovery) to SRRM3 (CAT#: L-016790–02), SRRM4 (CAT#: L-019322–02) or non-targeting control (CAT#: D-001810–10) using the TransIT-siQUEST Transfection Reagent (Mirus Bio) according to manufacturer's protocols. For all transient assays, cells were seeded 24 hours prior to transfections and total RNA or protein was collected 72 hours post-transfection.

For stable overexpression of ASCL1, lentiviral particles were generated and C4–2B cells were transduced at a multiplicity-of-infection of 4 with either the FU-CGW empty vector backbone or FU-ASCL1-CGW vector expressing ASCL1 (AddGene). ASCL1 cDNA (GenScript) was PCR amplified, purified, and cloned into the EcoRI site of the FU-CGW lentiviral backbone by NEBuilder HiFi DNA Assembly (New England Biolabs). 72 hours after lentiviral transduction, cells were trypsinized, collected as single cell suspensions, and placed into Advanced DMEM/F12 media supplemented with B27, 2 mM GlutaMAX (Gibco), and 10 ng/ml recombinant human basic FGF and EGF. Cells were cultured for 7 days prior to protein collection for immunoblot analysis.

Immunoblot analysis:

Protein from LuCaP PDX models and cell lines were obtained using the Nuclear Extract Kit (Active Motif) according to manufacturer's whole cell protein extracts protocols. Quantification of total protein was determined using the RcDc Protein Assay (Bio-Rad Laboratories) according to manufacturer's protocols. Thirty micrograms of total protein lysate were electrophoresed on 4–15% Bis-Tris gels (Bio-Rad Laboratories) with 1x Tris/Glycine/SDS Buffer (Bio-Rad Laboratories). The proteins were transferred to nitrocellulose membranes that were blocked with 5% Blotting-Grade Blocker (Bio-Rad Laboratories) in TBS/0.1% Tween-20 and subsequently probed with primary and secondary antibodies (Supplementary Table S2). Primary antibodies (AR, KLK3, SYP, ASCL1 and REST) have been validated and published previously using our LuCaP models, CRPC cell lines and patient specimens (7,27–29). For SRRM3 and SRRM4 antibodies, ectopic expression and siRNA studies conducted in this report provided positive and negative controls for additional

antibody validation. Proteins were visualized using Clarity Western ECL Substrate (Bio-Rad Laboratories).

Data availability:

Transcriptome analyses of the University of Washington Rapid Autopsy (UWRA) mCRPC, SU2C mCRPC, LuCaP PDX models and cell lines transfected with siRNAs to REST or a non-targeting control were conducted using previously published RNA sequencing datasets (7,30). The TCGA PanCancer and small cell lung cancer transcriptome datasets were accessed and analyzed through cBioPortal (31–33). RNA sequencing data and EPIC array methylation data generated in this report from mCRPC biospecimens and CRPC cell lines have been deposited at Gene Expression Omnibus (GEO) and can be accessed through accession number GSE158599 (https://www.ncbi.nlm.nih.gov/geo/query/acc.cgi?acc=GSE158599). The single cell RNA sequencing data from human MYCN mouse model ventral prostates were deposited on GEO and can be accessed through accession number GSE158468 (https://www.ncbi.nlm.nih.gov/geo/query/acc.cgi?acc=GSE158468). Details of experimental procedures for other methods including, RT-PCR, immunohistochemistry, RNA *in situ* hybridization, transcriptomic and epigenomic profiling, data analysis, and statistical analysis are included in the Supplementary Materials and Methods. Additionally, all primer set sequences and antibodies used in this report are listed in Supplementary Tables S1 and S2, respectively.

RESULTS

Alternative splicing of REST to REST4 variants is a hallmark of AMPC and SCNPC

To determine the landscape of REST splice variants in mCRPC, we conducted polymerase chain reaction (PCR) analysis using representative patient and LuCaP patient-derived xenograft (PDX) specimens from normal prostate (NP; n=5), ARPC (n=5), AMPC (n=5), ARLPC (n=5), DNPC (n=5) and SCNPC (n=4). The molecular phenotypes of the University of Washington Rapid Autopsy (UWRA) mCRPC biospecimens and LuCaP PDX models were identified previously (7). The literature suggests that the *REST* transcript could have up to 45 different splice variants (variants S1-S45) that are expressed in tissue- and context-dependent circumstances (34). However, we focused our analysis on all *REST* splice variants that include neuron-specific exon N3c using established PCR primers and protocols (34) (Figure 1A). PCR analysis in conjunction with amplicon sequencing confirmed that *REST* splice variants encoding full length REST proteins (exons 1a or 1b, 2, 3 and 4; variants S1 and S11) were detected in all specimens (Figure 1A and B). Further, *REST* splice variants with exon 2 skipping were also present in all specimens in conjunction with exon 1a (variant S5). While PCR analysis using primers for exon 1c (E1cF1/E4R1) detected faint bands in some mCRPC specimens, we could not confirm the presence of *REST* splice variants incorporating exon 1c through sequencing. In addition, neither PCR nor sequencing detected variants with exon 3 skipping that may encode REST proteins with diminished nuclear translocation (Figure 1A and B). However, this does not exclude exon 3 skipping as a potential mechanism for REST activity attenuation in NE^+ mCRPC. Importantly, we confirmed that exon N3c was present exclusively in AMPC and SCNPC specimens and that it was incorporated in multiple alternatively spliced *REST* transcripts that included either

exon 1a or 1b, or had exon 2 skipping (variants S3, S7 and S12; Figure 1A and B). Thus, our data suggests that alternative splicing of *REST* transcripts to variants encoding REST4 is a common event in mCRPC tumors with NE features. A summary of all confirmed *REST* splice variants identified in the 29 biospecimens are noted in Supplementary Table S3.

Next, we sought to identify other potential mechanisms capable of suppressing REST activity in mCRPC. While we verified the presence of *REST* splice variants that include exon N3c in AMPC and SCNPC specimens, the relative abundance of N3c variants in SCNPC tumor specimens were markedly lower compared to AMPC. RNA sequencing (RNAseq) from the UWRA mCRPC cohort determined that SCNPC tumors had significantly lower *REST* transcript expression ($p<0.0001$) compared to the other molecular phenotypes (Figure 1C). To ascertain if DNA methylation influenced *REST* and *AR* expression in SCNPC, we subjected the biospecimens used for PCR analysis to loci-specific methylation analysis using the EpigenDX platform. Predetermined CpGs along the *AR* locus and encompassing the *REST* transcriptional start site and 5'-untranslated region (UTR; i.e. exons 1a, 1b and 1c) showed no significantly altered methylation changes between mCRPC phenotypes (Supplementary Tables S4 and S5). However, methylated CpGs around the translational start site within *REST* exon 2 demonstrated significant ($p<0.05$) and progressive demethylation with loss of AR expression (Supplementary Table S5). Using an orthogonal approach, we employed EPIC array analysis to identify genome-wide methylated CpGs in ARPC C4–2B and SCNPC NCI-H660 cells. The *REST* locus contained a differentially methylated region (DMR) between the 5'UTR and exon 2, with increased DNA methylation detected in NCI-H660 cells (Figure 1D). Further, combination of methylated-DNA precipitation and methylation-sensitive restriction enzymes (COMPARE-MS) supported the observation of CpG hypermethylation of the *REST* DMR in SCNPC LuCaP PDX models compared to ARPC LuCaP PDX models (Figure 1E). Methylation within the *REST* DMR associated with *REST* transcript expression in 4 of the 5 SCNPC LuCaP PDX models (Figure 1F). Attenuated *REST* transcript expression did not appear to be correlated with methylation for LuCaP 49. Interestingly, SCNPC LuCaP 93 had low levels of DNA methylation and high expression levels of *REST* transcript. However, we previously confirmed that the principal *REST* transcripts expressed in LuCaP 93 encode REST4 and that REST activity is suppressed despite high *REST* transcript expression (7,21). Together, our data suggests that attenuation of REST activity regardless of AR status, either through alternative splicing or through reduced transcript expression, is a pivotal step for NE conversion in mCRPC.

SRRM3 is expressed in AMPC and SCNPC tumors and associates with attenuated REST activity

While characterizing the AMPC LuCaP 77CR PDX model (27), we noticed that not all 77CR tumors exhibited alternative splicing of *REST* transcripts to include exon N3c (Figure 2A). To scrutinize disparate 77CR tumors, we conducted immunoblot analysis of REST4-positive and REST4-negative 77CR tumor lysates (Figure 2B). We observed a REST isoform at 120 KDa and two isoforms at 200 KDa with our REST C-terminus antibody in LuCaP 77CR tumors. Comparatively, there were decreases in all three REST isoforms expressing the C-terminus repressor domain in the REST4-positive 77CR tumor (ET 232).

In addition, AR protein expression appeared similar between 77CR tumors, but SYP protein expression was drastically increased in the REST4-positive 77CR tumor, indicating loss of REST-mediated transcriptional repression. Furthermore, RNA-*in situ* hybridization (BaseScope) of additional 77CR tumor specimens using probes specific to *SRRM4* and *REST* exon N3c confirmed the heterogeneity of REST splicing in tumors with a subset of tumors positive for REST4 and a subset of tumors negative for REST4 (Figure 2C). Of note, *REST* exon N3c readouts were detected throughout the tumor cell population in REST4-positive tumors, suggesting that alternative splicing to REST4 was adopted by the majority of tumor cells. Strikingly, BaseScope analysis also revealed that *SRRM4* transcript expression was absent in REST4-positive LuCaP 77CR tumors (Figure 2C). Moreover, BaseScope substantiated our previous observations that the SCNPC LuCaP 93 PDX model had high transcript expression of *SRRM4* and *REST* exon N3c, and that ARPC LuCaP PDX models were negative for *SRRM4* and inclusion of *REST* exon N3c (Supplementary Figure S1A). Immunohistochemical (IHC) analysis of REST4-positive LuCaP 77CR PDX specimens determined that SYP and CHGA were uniformly and strongly expressed, whereas REST4-negative tumors expressed SYP and CHGA focally (Figure 2D). IHC for AR and prostate specific antigen (PSA/KLK3) revealed strong AR and PSA expression throughout tumor specimens irrespective of REST4 status. RNAseq of LuCaP 77CR tumors established that the *SRRM4* transcript was absent in all tumor specimens and that REST4-positive tumors had considerably higher expression of well characterized REST-repressed genes (*SYP, CHGA, SNAP25, SCG3*) compared to REST4-negative tumors (Figure 2E). As expected, genes associated with AR-active tumors (*AR, NKX3–1* and *KLK3*) were highly expressed and had similar expression levels in all 77CR tumors. Moreover, genes encoding transcription factors and drivers of the SCNPC phenotype (*SOX2, NKX2–1, POU3F2* and *LMO3*) had low expression in all 77CR tumor specimens. Furthermore, alignment data from the 77CR RNAseq profiles supported our previous PCR analyses and resolved REST splicing events around the 5'-UTR (exon 1a and 1b) irrespective of REST4 status but detected alternative splicing around exon N3c only in the REST4-positive tumors (Supplementary Figure S1B). These data suggest that NE differentiation and loss of REST activity in AMPC 77CR tumors are associated with alternative splicing and that a splicing factor distinct from SRRM4 is responsible for converting REST to REST4 in AMPC 77CR tumors.

To discover novel splicing factors contributing to the expression of REST-repressed transcripts, we conducted differential expression analysis between REST4-positive and REST4-negative 77CR biospecimens (Figure 3A). The top upregulated differentially expressed genes in REST4-positive 77CR tumors included *SYP*, *CHGA,* and several neurogenic molecules that are known to be REST-repressed in CRPC, including *CHGB, CHRNB2, VGF, UNC13A* and *CPLX2* (7,21). Notably, we identified upregulated *SRRM3* expression in REST4-positive 77CR tumors. While SRRM3 has been reported to be an RNA splicing factor important for vertebrate central nervous system development (35,36), its expression and activity in carcinogenesis and tumor progression are not defined. Thus, we used RNAseq to examine the expression of *SRRM3* and REST-repressed genes associated with *SRRM3* expression in ARPC and SCNPC LuCaP PDX models (Figure 3B). Importantly, *SRRM3* expression and REST-repressed genes were strongly upregulated in

SCNPC LuCaP PDX models and were absent in ARPC LuCaP PDX models. Additionally, immunoblot analysis of LuCaP PDX models determined that REST4-positive 77CR and SCNPC tumor specimens displayed robust SRRM3 protein expression, whereas ARPC tumors, REST4-negative 77CR and DNPC 173.2 did not express SRRM3 protein (Figure 3C).

We also examined the expression of SRRM3 and REST-repressed genes in AR-active C4–2B, VCaP and 22Rv1 CRPC cell lines and in AR-null SCNPC NCI-H660 cells. Transcriptome analysis determined that *SRRM3* and REST-repressed transcripts were upregulated in VCaP, 22Rv1 and NCI-H660 cells relative to C4–2B cells (Figure 3D). Of note, *SRRM4* transcript expression was upregulated in 22Rv1 cells only. Immunoblot analysis determined that REST protein with intact C-terminus repressor domain was considerably reduced in VCaP, 22Rv1 and NCI-H660 cells compared to C4–2B cells (Figure 3E). Mirroring the RNAseq data, SRRM3 and SYP proteins were detected in VCaP, 22Rv1 and NCI-H660 cells, and SRRM4 protein was detected in 22Rv1 cells only. In addition, we established that *REST* splice variants with exon N3c inclusion occurred intrinsically in VCaP, 22Rv1 and NCI-H660 cells (Figure 3F). Thus, attenuated REST activity and alternative splicing of REST to REST4 in VCaP and NCI-H660 cells occurs independent of SRRM4. Next, we examined the UWRA mCRPC RNAseq for *SRRM3* and *SRRM4* expression in ARPC, AMPC and SCNPC tumors. Although *SRRM3* and *SRRM4* transcripts were significantly upregulated in AMPC ($p<0.0001$) and SCNPC ($p<0.0001$) compared to ARPC, only *SRRM4* transcript expression was significantly higher ($p<0.05$) in SCNPC compared to AMPC (Figure 3G and H). Notably, *SRRM4* expression was more heterogeneous compared to *SRRM3* expression in AMPC and SCNPC specimens. Transcriptome analysis of the SU2C mCRPC cohort yielded similar results for *SRRM3* and *SRRM4* expression, but mean *SRRM3* expression was significantly higher ($p<0.05$) in SCNPC compared to AMPC (Supplementary Figure S2A and B). Together, these data further illustrate that VCaP and 22Rv1 cells are *in vitro* models of AMPC and suggest that SRRM3 is widely expressed across CRPC phenotypes with NE differentiation.

SRRM3 and SRRM4 alternatively splice REST transcripts and promote NE differentiation across tumor types

To interrogate SRRM3 function and establish REST as a direct target of SRRM3-mediated alternative splicing in CRPC, we ectopically expressed SRRM3 and SRRM4 in AR-active C4–2B and AR-null DU145 cells. PCR analysis confirmed that *REST* exon N3c expression was increased in both C4–2B and DU145 cells after transient transfection with either SRRM3 or SRRM4 (Figure 4A and B). Immunoblot verified that SRRM3 and SRRM4 proteins were expressed and that both SRRM3 and SRRM4 induced SYP protein expression in C4–2B cells (Figure 4A and B). Despite considerable SRRM3 and SRRM4 protein expression in DU145 cells, we were unable to detect corresponding increases in SYP protein. However, qPCR indicated that SRRM3 and SRRM4 ectopic expression bolstered the expression of REST-repressed genes in C4–2B cells, whereas only *SYP* expression was increased in DU145 cells (Supplementary Figure S3A and B). Congruently, we transfected AMPC 22Rv1 cells with siRNAs to SRRM3 (siSRRM3), SRRM4 (siSRRM4) or a non-targeting control (siNCT) and examined impacts on REST expression and function. While

ablated SRRM3 or SRRM4 protein alone increased full-length REST protein and inhibited SYP protein expression, knockdown of both SRRM3 and SRRM4 (siCombo) substantially rescued REST protein expressing the C-terminus repressor domain and markedly reduced SYP protein expression (Figure 4C). Interestingly, increased full-length REST expression after SRRM4 knockdown associated with decreased SRRM3 protein expression, suggesting that REST activity may regulate SRRM3 in CRPC cell lines. SRRM3/4 have been suggested to be under the transcriptional control of REST in breast cancer and neurogenesis (23,37). To determine if REST regulates SRRM3 in CRPC, we performed transcriptome analysis of AR-expressing and AR-null cell lines transfected with siRNA to REST (siREST) or a non-targeting siRNA (siNCT). REST knockdown in all cell lines led to upregulation of *SRRM3* expression and REST-repressed genes, whereas *SRRM4* expression was not altered (Supplementary Figure S3C). In search of other potential regulators of *SRRM3* expression, we used the C4–2B and NCI-H660 EPIC array data to identify DMRs encompassing the *SRRM3* locus. We identified hypermethylation of a DMR within the first intron of *SRRM3* that was associated with *SRRM3* expression in NCI-H660 cells (Supplementary Figure S3D). Additionally, COMPARE-MS analyses of ARPC and SCNPC LuCaP PDX models supported this observation and showed that hypermethylated CpGs within the DMR were associated with *SRRM3* expression in SCNPC (Supplementary Figure S3E). To further investigate this association, we performed motif and transcription factor binding site analyses using the MEME Suite TomTom tool (38) and observed that regulatory sequences associated with *PRDM6*, *PAX5* and *AR* binding were significantly enriched in the *SRRM3* DMR sequence.

To identify other targets of SRRM3-mediated alternative splicing, we examined alternative splice variants of *LSD1/KDM1A* and *BHC80/PHF21A* that are induced by SRRM4 activity and contribute to NE conversion (39,40). PCR analysis determined that inclusion of exon 8a in *LSD1* transcripts as well as exon 14a from the mutually exclusive exons 14 and 14a in *BHC80*, were increased in C4–2B and DU145 cells ectopically expressing SRRM3 and SRRM4 (Figure 4D, E and Supplementary Figure S3F). These data demonstrate that SRRM3 and SRRM4 can have analogous functions in CRPC.

To examine the broader biological impacts associated with SRRM3 and SRRM4 expression in AR-expressing and AR-null CRPC models, we subjected C4–2B and DU145 cells ectopically expressing SRRM3 or SRRM4 to RNAseq and gene set enrichment analysis (GSEA). Transcriptome analysis showed that either SRRM3 or SRRM4 expression in C4–2B cells resulted in significant upregulation (up>1.5 fold, $p<0.05$) of known REST-repressed genes, including *SYP, SNAP25, UNC13A, CHRNB2* and *SCG3* (Figure 5A and Supplementary Figure S4A). Moreover, there were no significant alterations in expression of *AR* and *AR* associated genes or SCNPC transcription factors *SOX2, NKX2–1, POU3F2* and *LMO3*. Of the 146 significantly upregulated genes in C4–2B cells expressing SRRM3 and of the 107 significantly upregulated genes in C4–2B cells expressing SRRM4, there were 45 upregulated genes in common (Figure 5B). Conversely, the DU145 cells were less amenable to SRRM3 and SRRM4 expression as few REST-repressed genes were significantly upregulated (up>1.5 fold, $p<0.05$; Figure 5A and Supplementary Figure S4B). Of all gene transcripts significantly upregulated (up>1.5 fold, $p<0.05$) in DU145 cells expressing SRRM3 (n=129) or SRRM4 (n=187), 9 genes were in common between SRRM3

and SRRM4 (Figure 5B). While the 5 unanimously upregulated genes in both cell lines expressing SRRM3 or SRRM4 were REST-repressed genes (*SYP, PAX5, UNC13A, VGF, RAB39A*), *CHGA* was not significantly altered by SRRM3 or SRRM4 expression in either cell line, suggesting a multifactorial regulatory mechanism (Supplementary Table S6). GSEA of all significantly altered genes (FDR<0.05) using the MSigDB C3-Transcription Factor Target database identified the REST pathway as the top significantly altered pathway in both C4–2B cells and DU145 cells expressing either SRRM3 or SRRM4, indicating that inactivation of REST repression is a primary function of SRRM3 and SRRM4 activity (Supplementary Figure S4C). Gene ontology using the Cellular Component pathways determined that SRRM3 and SRRM4-expressing cells had increased normalized enrichment scores (NES) for pathways controlling synaptic vesicle formation, transport and release (Figure 5C). Thus, despite AR expression and activity in C4–2B cells, SRRM3 or SRRM4 alone is sufficient for inducing biological pathways that control neuronal secretory functions that are typical of NE^+ CRPC cells. These GSEA results were recapitulated in LuCaP 77CR tumors with high *SRRM3* expression, strongly supporting the physiological relevance of our approach (Figure 5D). Together, our data indicate that SRRM3 and SRRM4 drive conversion of ARPC to AMPC through alternative splicing and attenuation of REST and that expression of either splicing factor alone is not sufficient for complete SCNPC conversion *in vitro*.

To glean further biological insights into SRRM3 expression in other tumor types, we queried The Cancer Genome Atlas (TCGA) Pan-Cancer RNAseq datasets. Of the 32 cancer datasets, adrenocortical carcinoma (ACC), pheochromocytoma and paraganglioma (PCPG) and uveal melanoma had the highest median *SRRM3* expression (Supplementary Figure S5A). On the other hand, PCPG, low grade gliomas (LGG), and glioblastoma multiforme (GBM) had the highest median *SRRM4* expression (Supplementary Figure S5B). Furthermore, we stratified transcriptome profiles from small cell lung cancer (SCLC) tumors based on high and low *SRRM3* expression (Supplementary Figure S6; Ref. (33)). Importantly, we determined that $SRRM3^{high}$ SCLC had significant upregulation of *SRRM4* ($p=6.34\times10^{-4}$), *SYP* ($p=7.80\times10^{-7}$), *CHGA* ($p=1.21\times10^{-7}$), *SNAP25* ($p=1.31\times10^{-7}$) and *UNC13A* ($p=2.29\times10^{-7}$), while *REST* expression was significantly decreased ($p=3.14\times10^{-9}$). Together, these data strongly suggest that SRRM3 activity and REST attenuation are key to neural crest-derived tumors and exacerbate NE biology in SCLC.

To determine if Srrm3 and Srrm4 are expressed in murine PC cells, we employed transcriptome analysis using a genetically engineered mouse model (GEMM) expressing human MYCN (*Pb-Cre+; Pten$^{f/f}$; MYCN+; Rb1$^{f/f}$*). RNAseq of ventral prostate tumors revealed that *Srrm3* and *Srrm4* expression were significantly upregulated ($p<0.05$) in poorly differentiated tumors from both castrated and intact mice compared to adenocarcinomas from intact mice (Supplementary Figure S7). Next, we conducted single cell RNA sequencing (scRNAseq) to more clearly identify cell populations that expressed *Srrm3* and *Srrm4* (Figure 6A). The scRNAseq of 8-week-old ventral prostates (n=3) revealed distinct populations of *MYCN* expressing cells, including a subpopulation expressing SCNPC features (*Ar*$^-$ and *MYCN*$^+$, *Syp*$^+$ or *ChgA*$^+$ or *Insm1*$^+$; Figure 6B, Supplementary Figure S8A). Importantly, cells with *Srrm3* or *Srrm4* expression or *Srrm3* and *Srrm4* co-expression clustered with the SCNPC-like cell cluster (Figure 6C–E). Differential

expression analysis between *Srrm3*$^+$ or *Srrm4*$^+$ SCNPC-like cells and ARPC-like cells (i.e. *Ar*$^+$ and *Syp*$^-$) and Enrichr gene ontology (GO) analysis of significantly altered genes ($p<0.05$) determined that nervous system development ($p=9.37\times10^{-15}$) was the top enriched pathway in *Srrm3*$^+$ or *Srrm4*$^+$ SCNPC-like cells compared to ARPC-like cells (Figure 6F and Supplementary Table S7). Additionally, AMPC-like cells (i.e. *Ar*$^+$/*Syp*$^+$) have been reported in CRPC GEMM models but the molecular events leading to this cellular state are not well understood (11,41). We detected *Srrm3*$^+$ and *Srrm4*$^+$ cells with AMPC-like profiles in the scRNAseq data (Supplementary Figure S8B–D). Moreover, AMPC-like cells demonstrated significant ($p<0.05$) upregulation of REST-repressed genes compared to ARPC-like cells (Supplementary Figure S8E). In agreement with C4–2B and LuCaP 77CR results from Figure 5, Enrichr GO analysis determined that chemical and synaptic transmission ($p=1.54\times10^{-19}$) was the top enriched pathway for differentially expressed genes ($p<0.05$) in AMPC-like cells compared to ARPC-like cells (Supplementary Figure S8F and Supplementary Table S8). These data indicate that attenuation of REST activity via *Srrm3* and *Srrm4* expression occurs in *Ar*$^-$ and *Ar*$^+$ cells with NE differentiation in a CRPC GEMM model. In addition, the AMPC molecular phenotype is not unique to human CRPC cells.

SRRM3 and SRRM4 expression delineate diverse biological classes of AMPC and SCNPC

The transcriptome analyses of the UWRA and SU2C mCRPC cohorts demonstrated that *SRRM3* was upregulated in the majority of AMPCs but not all, and that *SRRM4* expression was more robust in SCNPCs compared to AMPCs (Figure 3G, H and Supplementary Figure 2A and B). These findings suggest that *SRRM3* and *SRRM4* could stratify mCRPC biospecimens with biologically distinct NE programs. Thus, we scrutinized the SU2C mCRPC polyA RNAseq dataset (n=270; Ref. (30)) as well as transcriptomes from the UWRA mCRPC and LuCaP PDX models and focused on transcription factors driving differentiation states. First, we segregated tumor transcriptional profiles based on the expression of luminal fate transcription factors and biomarkers (*AR, NKX3–1, KLK2, KLK3, TARP*) and broadly expressed NE biomarkers (*SYP, CHGA, CHGB, SCG3, SEZ6*) and this revealed ARPC, AMPC, ARLPC, DNPC and SCNPC molecular phenotypes across all datasets (Supplementary Figure S9 and Supplementary Figure S10A and B). Next, we stratified AMPC tumors in the SU2C/UWRA datasets using *SRRM3* and *SRRM4* expression and identified AMPC tumors with *SRRM3/4* expression and AMPC tumors without *SRRM3/4* expression (Figure 7A and B). Notably, AMPC tumors typically expressed *SRRM3* transcript alone or in conjunction with *SRRM4* but not *SRRM4* alone (Figure 7A and B). As expected, differential expression analysis between ARPC tumors and AMPC-*SRRM3*$^+$ tumors in the SU2C dataset revealed that significantly upregulated genes (FDR<0.05, $\log_2$FC>1) in AMPC-*SRRM3*$^+$ tumors included REST-repressed genes (*ACTL6B, CHRNB2, SNAP25, UNC13A, XKR7*) and broad NE biomarkers (Supplementary Figure S11A). However, differential expression analysis in the SU2C dataset between ARPC and *SRRM3/4*-null AMPC tumors revealed *ASCL1* as the top differentially expressed gene (FDR<0.05, $\log_2$FC>1; Supplementary Figure S11B). Interestingly, the majority of REST-repressed genes associated with *SRRM3* expression were not altered in AMPC-*ASCL1*$^+$ (SRRM3/4-null) mCRPC tumors. To determine if ASCL1 could drive an alternative AMPC phenotype, we stably expressed ASCL1 in C4–2B

cells and examined genes associated with AMPC-*ASCL1*$^{+}$ tumor specimens. Immunoblot analysis demonstrated that ASCL1 induced SYP and INSM1 protein expression, whereas SRRM3, SRRM4 and full-length REST proteins were not altered (Figure 7C). Moreover, AR protein expression and activity (STEAP1) remained intact, suggesting that C4–2B cells expressing ASCL1 acquire the molecular features of AMPC-*ASCL1*$^{+}$ patient tumors.

While characterizing *SRRM3* and *SRRM4* expression in AMPC tumors in the SU2C and UWRA datasets, we also observed that SCNPC tumors typically expressed *SRRM3*, whereas *SRRM4* expression was limited to a subset of SCNPC tumors and was associated with *MYCN* expression (Figure 7A and B). Differential expression analysis between SCNPC tumors lacking SRRM4 expression (SCNPC-1) and ARPC in the SU2C dataset revealed that REST-repressed genes and *ASCL1* were the top significantly upregulated genes (FDR<0.05, $\log_2$FC>1) in SCNPC-1 (Supplementary Figure S11C). Of note, the NEUROD basic-Helix-Loop-Helix (bHLH) transcription factor family (*NEUROD1, NEUROD2, NEUROD4, NEUROD6*) have various functions in neuronal fate, and NeuroD1 specifically classifies a subset of SCLC tumors (42,43). While *NEUROD1* and *NEUROD4* were expressed in *SRRM4/MYCN* expressing SCNPC tumors in the SU2C dataset, only a subset of *SRRM4/MYCN* tumors expressed *NEUROD6* transcript (Figure 7A and B). Differential expression analysis between ARPC and SCNPC tumors with upregulated *SRRM4, MYCN, NEUROD1* and *NEUROD4* (SCNPC-2) revealed significantly upregulated neural transcription factors (FDR<0.05; $\log_2$FC>1) such as *ZNF536, ISL1, PAX6* and *MYT1L* (Supplementary Figure S11D). Conversely, differentially expressed genes between ARPC and SCNPC tumors expressing *NEUROD6* (SCNPC-3) in the SU2C dataset identified *BARHL1, LHX3, UNCX, POU3F3, POU4F2, POU4F3* and *ATOH1* as significantly upregulated (FDR<0.05, $\log_2$FC>1) neural transcription factors in SCNPC-3 tumors (Supplementary Figure S11E). Notably, *POU4F3* and *ATOH1* were not highly expressed in SCNPC-3 in the UWRA or LuCaP PDX datasets; however, this observation is based on a single mCRPC sample, and the PDX line was derived from this same metastasis. Nevertheless, for all three SCNPC molecular phenotypes the expression of a set of defined transcription factors were recapitulated in all three RNAseq datasets.

Next, we examined the expression of transcription factors *SOX2*, *PROX1*, *LHX2* and *LMO3* that have been reported to be upregulated in SCNPC (7,44,45). While *SOX2*, *PROX1*, *LHX2* and *LMO3* were generally expressed in SCNPC tumors, *SOX2* and *PROX1* also demonstrated marked expression in transitioning/mixed DNPC tumors (i.e. NE^{low}; Figure 7A and B). Finally, we assessed the expression of neural cell surface antigens *NCAM1, NRCAM* and *L1CAM* and determined that SCNPC generally upregulated the expression of all antigens (Figure 7A and B). Together, these data suggest that *PROX1* and *SOX2* are expressed in early NE differentiation programs and further support that *NCAM1* is a useful biomarker for metastatic SCNPC in CRPC (46,47).

To associate biological programs in NE^{+} mCRPC tumors expressing diverse transcription factors, we conducted GSEA using all significantly altered genes (FDR<0.05) compared to ARPC for AMPC-*SRRM3*$^{+}$, AMPC-*ASCL1*$^{+}$, SCNPC-1, SCNPC-2 and SCNPC-3. Analysis of the Hallmark pathways demonstrated that genes contributing to mitotic spindle, G2M checkpoint and E2F targets were significantly enriched compared to ARPC

in AMPC-*SRRM3*$^+$, SCNPC-1 and SCNPC-2, but were diminished in AMPC-*ASCL1*$^+$ and SCNPC-3 (Figure 7D). These data suggest that the proliferative capacity of NE$^+$ phenotypes may be different, but larger cohorts are needed to confirm these observations. Congruently, the LuCaP 173.1 PDX model recapitulates SCNPC-3 and tumor growth is slower when compared to other SCNPC LuCaP PDX models, noting that LuCaP 173.1 represents our only PDX model with this phenotype (Supplementary Figure S12A and B). Likewise, GSEA of the GO Biological Process pathways demonstrated that the top enriched pathways for SCNPC-1 were involved in cell-cycle and proliferation, whereas SCNPC-2 and SCNPC-3 were enriched for highly differentiated neuronal pathways (Supplementary Table S9). Importantly, SCNPC-3 tumors displayed enrichment for multiple GO Biological Process pathways involved in sensory neuron biology and glutamate signaling, indicating a more neuronally differentiated phenotype compared to SCNPC-1 tumors. Shared and unique upregulated genes (FDR<0.05, $\log_2$FC>2) in SCNPC-1, SCNPC-2 and SCNPC-3 validated the transcription factors defining the molecular subtypes (Figure 7E and Supplementary Table S10). Conversely, GO Biological Process pathways revealed that AMPC-*SRRM3*$^+$ and AMPC-*ASCL1*$^+$ were both enriched for overlapping pathways involving neurotransmitter and synaptic vesicle regulation (Supplementary Table S11). However, significantly upregulated genes (FDR<0.05, $\log_2$FC>2) encoding secreted neurogenic molecules and synaptic vesicle proteins were shared between AMPC-*SRRM3*$^+$ and AMPC-*ASCL1*$^+$ (Figure 7F and Supplementary Table S12). These data indicate that the AMPC phenotype can arise through convergent biological pathways regulated by REST or ASCL1. Moreover, SCNPC may exist as a spectrum with de-differentiated and rapidly proliferating tumors (SCNPC-1) potentially leading to more differentiated SCNPC tumors resembling glutamatergic sensory neurons (SCNPC-3).

DISCUSSION

Widespread and long-term use of AR signaling inhibitors are changing the molecular and phenotypic landscapes of PC. In addition, cellular plasticity and the emergence of novel mCRPC phenotypes has led to new and evolving features of mCRPC biology. We and others have identified dysregulation of the REST pathway as a critical step for treatment-resistance and NE differentiation in PC (7,18–21). However, the molecular underpinnings of REST regulation in clinical mCRPC specimens and the relationship of attenuated REST activity to the spectrum NE tumor types were not well understood. In this report, we used mCRPC biospecimens and LuCaP PDX models to characterize REST alternative splice variants across ARPC, AMPC, ARLPC, DNPC and SCNPC phenotypes (7). Our approach identified alternative splicing of REST to REST4 and DNA methylation of the *REST* locus as key biological mechanisms contributing to attenuated REST activity in mCRPC tumors with NE features. In support of our data, *REST* methylation, reduced *REST* mRNA expression and the expression of REST4 splice variants are noted in SCLC (22,48). However, SRRM4 has been reported as the principal RNA splicing factor responsible for inserting exon N3C to the *REST* transcript and converting REST to REST4 variants outside of the central nervous system (23,49,50). Importantly, we discovered SRRM3 expression in AMPC and SCNPC tumors and leveraged *in vitro* functional studies and transcriptome analyses to demonstrate that SRRM3 has overlapping functions with SRRM4 and alternatively splices REST to

REST4. In addition, we confirmed that SRRM3 expression and activity extends across NE cancer subtypes and in a SCNPC mouse model that expresses human MYCN. Altogether, our data greatly expands the biological significance of REST attenuation in tumors with NE differentiation and identifies diverse mechanisms regulating REST activity.

A major goal of the present study was to characterize *SRRM3* expression across tumor types and use upregulation of REST-repressed genes as a surrogate for SRRM3 function. This approach was supported through our *in vitro* experiments validating that SRRM3 and SRRM4 induce alternative REST splicing and upregulation of REST-repressed genes in CRPC. Although stable expression of SRRM4 has previously been shown to induce SYP protein expression and transdifferentiation of DU145 cells to a SCNPC-like phenotype (51), we were unable to recapitulate SCNPC progression in DU145 cells using a transient system. While we confirmed that both SRRM3 and SRRM4 induced alternative splicing of REST, LSD1 and BHC80 to neuronally expressed variants in C4–2B and DU145 cells, we speculate that epigenomic alterations in DU145 cells require further engagement for complete SCNPC transdifferentiation. Nevertheless, our analysis of transcriptome datasets in CRPC tumors and cell lines, SCLC and in a GEMM model of CRPC suggest that the vast majority of NE^+ cells upregulate *SRRM3* expression and attenuate REST activity to initiate cellular transformation. Indeed, SCNPC NCI-H660 cells have intrinsic REST4 expression and express SRRM3 only. Importantly, our data provides evidence that the AMPC phenotype could be a biological midpoint between the ARPC to SCNPC disease continuum and that SRRM3 is preferentially expressed in AR-active tumors and earlier in disease progression compared to SRRM4. In support of this hypothesis, we demonstrated that SRRM3 and SRRM4 expression are upregulated in neural crest cell tumors (ACC, PGPL, GBM, LGG and uveal melanoma) in the TCGA PanCancer dataset. Interestingly, the transcriptomes of the neural crest derived tumors cluster together and a 15 gene signature common to all tumors includes *SYP, CHGB, STMN3, BEX1, EEF1A2* (52). These genes were identified as significantly upregulated in C4–2B cells expressing SRRM3/SRRM4 and through differential expression analysis in the SRRM3-expressing LuCaP 77CR tumors. In addition, alternative REST splicing and REST4 variants have been observed in neuroblastoma, pheochromocytoma and glioma (53,54). Thus, our data cumulatively supports that de-differentiation to a neural crest cell state is likely a common event in advanced treatment-resistant tumors with the capacity for NE differentiation.

Small cell NE tumors across cancer types share common molecular features and therapeutic vulnerabilities (44,55). However, our dissection of transcription factors and biological pathways contributing to NE differentiation suggest that a more complex NE biology should be appreciated for therapeutic considerations. Indeed, we validated VCaP and 22Rv1 cells as *in vitro* models of AMPC. While both cell lines express the clinically relevant NE biomarkers SYP and CHGA, alternatively splice REST to REST4 and upregulate REST repressed neurogenic molecules, these cell lines have long been considered *in vitro* models of ARPC. Although VCaP cells respond to AR pathway inhibitors (56), 22Rv1 cells have markedly reduced PSA expression and are refractory to enzalutamide (57). How these molecular features relate to treatment-response in the patient population will require further investigation. In parallel, transcriptome analysis using the SU2C and UWRA mCRPC specimens and the LuCaP PDX models identified molecular subsets of AMPC and SCNPC

that greatly inform the biology of NE transdifferentiation. We recognize that the number of SCNPC tumors within the SU2C, UWRA and LuCaP PDX model transcriptome datasets are relatively small and further validation of our findings will be required. Additionally, the potential examination of mixed tumor cell populations inherent to bulk RNAseq, the temporal considerations of single biopsies and the issues of multifactor regulation for some NE biomarkers (eg. CHGA) need to be appreciated. However, the consistency of transcription factor profiles across multiple mCRPC datasets lends strength to our analysis. Principally, we characterized two AMPC phenotypes driven by either REST attenuation or ASCL1 activity and three progressively neuronal SCNPC phenotypes characterized by (i) *SRRM3* and *ASCL1* expression only (SCNPC-1), (ii) *SRRM3, SRRM4*, *MYCN* and *NEUROD1* expression (SCNPC-2) and (iii) *SRRM3*, *SRRM4*, *MYCN* and *NEUROD6* expression (SCNPC-3; Supplementary Figure S13). Congruently, molecular phenotypes of SCLC can be distinguished by ASCL1 and NEUROD1 activity and it has been shown that SCLC can progress from an ASCL1 phenotype to a NEUROD1 phenotype through MYC activity (42,43,58). Additionally, ASCL1 activity can drive neuroendocrine reprogramming in some CRPC models (29). While SCNPC-2 tumors could be transitioning to SCNPC-3 tumors that resemble glutamatergic sensory neurons, our data suggests that the biology of SCNPC-1 tumors are strikingly different from SCNPC-2 and SCNPC-3 and could respond differently to therapies. For example, a recent clinical trial using the aurora kinase A inhibitor alisertib in SCNPC did not meet its primary endpoint of 6-month radiographic progression-free survival (59). However, the study identified a subset of responders and nominated MYCN overactivity as a biomarker for therapeutic benefit. While future testing of alisertib in stratified SCNPC preclinical models is needed, our data predict that SCNPC-1 tumors (MYCN-null) would be refractory to alisertib therapy. Thus, our profiling efforts delineate the heterogeneity observed in the SCNPC patient population and could be translated to future clinical trials for more appropriate patient selection.

In summary, our data highlight an unrecognized mechanism of ARPC to AMPC or SCNPC conversion that hinges on a SRRM3-REST regulatory axis. In addition, AMPC and SCNPC encompass multiple molecular phenotypes with convergent NE differentiation pathways. Future studies examining the pathology of novel NE^+ molecular subtypes would shed further light on the clinical impacts of diverse tumor characteristics. In the meantime, SRRM3 and SRRM4 could be used as biomarkers to distinguish distinct NE^+ phenotypes to aid in clinical trial design and patient tumor stratification.

Supplementary Material

Refer to Web version on PubMed Central for supplementary material.

ACKNOWLEDGEMENTS

We thank the patients and their families, Celestia Higano, Evan Yu, Elahe Mostaghel, Heather Cheng, Mike Schweizer, Bruce Montgomery, Funda Vakar-Lopez, Martine Roudier and the rapid autopsy teams in the Urology and Laboratory Medicine & Pathology Departments at the University of Washington. We would also like to thank the Animal Facility and the Comparative Medicine Animal Caregivers for assistance with the LuCaP PDX work. This work was supported by a Department of Defense Idea Development Award-Partnering-PI (W81XWH-17-1-0414; W81XWH-17-1-0415; M.P. Labrecque, L.G. Brown, I.M. Coleman, B. Lakely, H.M. Nguyen, D. Li, L.D. True, H.M. Lam, E. Corey, P.S. Nelson, and C. Morrissey), Department of Defense Idea

Award (W81XWH2010405; J.J. Alumkal), R01 CA251245 (J.J. Alumkal), NCI Drug Resistance and Sensitivity Network (P50 CA186786-07S1; J.J. Alumkal), R01 CA234715 (I.M. Coleman, D. Li, P.S. Nelson), the Pacific Northwest Prostate Cancer SPORE (P50CA97186; M.P. Labrecque, L.G. Brown, I.M. Coleman, B. Lakely, H.M. Nguyen, D. Li, L.D. True, D.W. Lin, H.M. Lam, J.J. Alumkal, E. Corey, P.S. Nelson, and C. Morrissey), the Department of Defense Prostate Cancer Biorepository Network (W81XWH-14-2-0183; L.G. Brown, B. Lakely, H.M. Nguyen, L.D. True, H.M. Lam, E. Corey, and C. Morrissey), Scientific Computing Infrastructure at Fred Hutch funded by ORIP (S10OD028685; I.M. Coleman, B. Hanratty), P01 CA163227 (I.M. Coleman, P.S. Nelson), P30 CA015704 (I.M. Coleman, D. Li, P.S. Nelson), U.S. Department of Defense Prostate Cancer Research Program (W81XWH-20-1-0111; M.C. Haffner), the Safeway Foundation (M.C. Haffner), the STTR (I.M. Coleman, B. Hanratty, P.S. Nelson), Institute for Prostate Cancer Research (M.P. Labrecque, L.G. Brown, I.M. Coleman, B. Lakely, H.M. Nguyen, L.D. True, D.W. Lin, E. Corey, P.S. Nelson, and C. Morrissey), and the Richard M. LUCAS Foundation (H.M. Nguyen and E. Corey).

REFERENCES

1. Lallous N, Volik SV, Awrey S, Leblanc E, Tse R, Murillo J, et al.Functional analysis of androgen receptor mutations that confer anti-androgen resistance identified in circulating cell-free DNA from prostate cancer patients. Genome biology2016;17:10 [PubMed: 26813233]
2. Sharp A, Coleman I, Yuan W, Sprenger C, Dolling D, Rodrigues DN, et al.Androgen receptor splice variant-7 expression emerges with castration resistance in prostate cancer. J Clin Invest2019;129:192–208 [PubMed: 30334814]
3. Takeda DY, Spisak S, Seo JH, Bell C, O'Connor E, Korthauer K, et al.A Somatically Acquired Enhancer of the Androgen Receptor Is a Noncoding Driver in Advanced Prostate Cancer. Cell2018;174:422–32 e13 [PubMed: 29909987]
4. Puhr M, Hoefer J, Eigentler A, Ploner C, Handle F, Schaefer G, et al.The Glucocorticoid Receptor Is a Key Player for Prostate Cancer Cell Survival and a Target for Improved Antiandrogen Therapy. Clinical cancer research : an official journal of the American Association for Cancer Research2018;24:927–38 [PubMed: 29158269]
5. Bluemn EG, Coleman IM, Lucas JM, Coleman RT, Hernandez-Lopez S, Tharakan R, et al.Androgen Receptor Pathway-Independent Prostate Cancer Is Sustained through FGF Signaling. Cancer cell2017;32:474–89 e6 [PubMed: 29017058]
6. Beltran H, Prandi D, Mosquera JM, Benelli M, Puca L, Cyrta J, et al.Divergent clonal evolution of castration-resistant neuroendocrine prostate cancer. Nature medicine2016;22:298–305
7. Labrecque MP, Coleman IM, Brown LG, True LD, Kollath L, Lakely B, et al.Molecular profiling stratifies diverse phenotypes of treatment-refractory metastatic castration-resistant prostate cancer. J Clin Invest2019;130:4492–505
8. Epstein JI, Amin MB, Beltran H, Lotan TL, Mosquera JM, Reuter VE, et al.Proposed morphologic classification of prostate cancer with neuroendocrine differentiation. The American journal of surgical pathology2014;38:756–67 [PubMed: 24705311]
9. Vlachostergios PJ, Puca L, Beltran H. Emerging Variants of Castration-Resistant Prostate Cancer. Curr Oncol Rep2017;19:32 [PubMed: 28361223]
10. Beltran H, Rickman DS, Park K, Chae SS, Sboner A, MacDonald TY, et al.Molecular characterization of neuroendocrine prostate cancer and identification of new drug targets. Cancer discovery2011;1:487–95 [PubMed: 22389870]
11. Ku SY, Rosario S, Wang Y, Mu P, Seshadri M, Goodrich ZW, et al.Rb1 and Trp53 cooperate to suppress prostate cancer lineage plasticity, metastasis, and antiandrogen resistance. Science2017;355:78–83 [PubMed: 28059767]
12. Lee JK, Phillips JW, Smith BA, Park JW, Stoyanova T, McCaffrey EF, et al.N-Myc Drives Neuroendocrine Prostate Cancer Initiated from Human Prostate Epithelial Cells. Cancer cell2016;29:536–47 [PubMed: 27050099]
13. Bishop JL, Thaper D, Vahid S, Davies A, Ketola K, Kuruma H, et al.The Master Neural Transcription Factor BRN2 Is an Androgen Receptor-Suppressed Driver of Neuroendocrine Differentiation in Prostate Cancer. Cancer discovery2017;7:54–71 [PubMed: 27784708]
14. Mu P, Zhang Z, Benelli M, Karthaus WR, Hoover E, Chen CC, et al.SOX2 promotes lineage plasticity and antiandrogen resistance in TP53- and RB1-deficient prostate cancer. Science2017;355:84–8 [PubMed: 28059768]

15. Dardenne E, Beltran H, Benelli M, Gayvert K, Berger A, Puca L, et al.N-Myc Induces an EZH2-Mediated Transcriptional Program Driving Neuroendocrine Prostate Cancer. Cancer cell2016;30:563–77 [PubMed: 27728805]
16. Nyquist MD, Corella A, Coleman I, De Sarkar N, Kaipainen A, Ha G, et al.Combined TP53 and RB1 Loss Promotes Prostate Cancer Resistance to a Spectrum of Therapeutics and Confers Vulnerability to Replication Stress. Cell reports2020;31:107669
17. Aggarwal R, Huang J, Alumkal JJ, Zhang L, Feng FY, Thomas GV, et al.Clinical and Genomic Characterization of Treatment-Emergent Small-Cell Neuroendocrine Prostate Cancer: A Multi-institutional Prospective Study. Journal of clinical oncology : official journal of the American Society of Clinical Oncology2018;36:2492–503 [PubMed: 29985747]
18. Flores-Morales A, Bergmann TB, Lavallee C, Batth TS, Lin D, Lerdrup M, et al.Proteogenomic Characterization of Patient-Derived Xenografts Highlights the Role of REST in Neuroendocrine Differentiation of Castration-Resistant Prostate Cancer. Clinical cancer research : an official journal of the American Association for Cancer Research2019;25:595–608 [PubMed: 30274982]
19. Lapuk AV, Wu C, Wyatt AW, McPherson A, McConeghy BJ, Brahmbhatt S, et al.From sequence to molecular pathology, and a mechanism driving the neuroendocrine phenotype in prostate cancer. The Journal of pathology2012;227:286–97 [PubMed: 22553170]
20. Svensson C, Ceder J, Iglesias-Gato D, Chuan YC, Pang ST, Bjartell A, et al.REST mediates androgen receptor actions on gene repression and predicts early recurrence of prostate cancer. Nucleic acids research2014;42:999–1015 [PubMed: 24163104]
21. Zhang X, Coleman IM, Brown LG, True LD, Kollath L, Lucas JM, et al.SRRM4 Expression and the Loss of REST Activity May Promote the Emergence of the Neuroendocrine Phenotype in Castration-Resistant Prostate Cancer. Clinical cancer research : an official journal of the American Association for Cancer Research2015;21:4698–708 [PubMed: 26071481]
22. Coulson JM, Edgson JL, Woll PJ, Quinn JP. A splice variant of the neuron-restrictive silencer factor repressor is expressed in small cell lung cancer: a potential role in derepression of neuroendocrine genes and a useful clinical marker. Cancer Res2000;60:1840–4 [PubMed: 10766169]
23. Raj B, O'Hanlon D, Vessey JP, Pan Q, Ray D, Buckley NJ, et al.Cross-regulation between an alternative splicing activator and a transcription repressor controls neurogenesis. Molecular cell2011;43:843–50 [PubMed: 21884984]
24. Chen GL, Miller GM. Alternative REST Splicing Underappreciated. eNeuro2018;5
25. Morrissey C, Roudier MP, Dowell A, True LD, Ketchanji M, Welty C, et al.Effects of androgen deprivation therapy and bisphosphonate treatment on bone in patients with metastatic castration-resistant prostate cancer: results from the University of Washington Rapid Autopsy Series. Journal of bone and mineral research : the official journal of theAmerican Society for Bone and Mineral Research2013;28:333–40
26. Roudier MP, True LD, Higano CS, Vesselle H, Ellis W, Lange P, et al.Phenotypic heterogeneity of end-stage prostate carcinoma metastatic to bone. Human pathology2003;34:646–53 [PubMed: 12874759]
27. Nguyen HM, Vessella RL, Morrissey C, Brown LG, Coleman IM, Higano CS, et al.LuCaP Prostate Cancer Patient-Derived Xenografts Reflect the Molecular Heterogeneity of Advanced Disease an--d Serve as Models for Evaluating Cancer Therapeutics. The Prostate2017;77:654–71 [PubMed: 28156002]
28. Brady L, Kriner M, Coleman I, Morrissey C, Roudier M, True LD, et al.Inter- and intra-tumor heterogeneity of metastatic prostate cancer determined by digital spatial gene expression profiling. Nature communications2021;12:1426
29. DeLucia DC, Cardillo TM, Ang L, Labrecque MP, Zhang A, Hopkins JE, et al.Regulation of CEACAM5 and Therapeutic Efficacy of an Anti-CEACAM5-SN38 Antibody-drug Conjugate in Neuroendocrine Prostate Cancer. Clinical cancer research : an official journal of the American Association for Cancer Research2021;27:759–74 [PubMed: 33199493]
30. Abida W, Cyrta J, Heller G, Prandi D, Armenia J, Coleman I, et al.Genomic correlates of clinical outcome in advanced prostate cancer. Proc Natl Acad Sci U S A2019;116:11428–36 [PubMed: 31061129]

31. Cerami E, Gao J, Dogrusoz U, Gross BE, Sumer SO, Aksoy BA, et al.The cBio cancer genomics portal: an open platform for exploring multidimensional cancer genomics data. Cancer discovery2012;2:401–4 [PubMed: 22588877]
32. Gao J, Aksoy BA, Dogrusoz U, Dresdner G, Gross B, Sumer SO, et al.Integrative analysis of complex cancer genomics and clinical profiles using the cBioPortal. Sci Signal2013;6:pl1
33. George J, Lim JS, Jang SJ, Cun Y, Ozretic L, Kong G, et al.Comprehensive genomic profiles of small cell lung cancer. Nature2015;524:47–53 [PubMed: 26168399]
34. Chen GL, Miller GM. Extensive alternative splicing of the repressor element silencing transcription factor linked to cancer. PloS one2013;8:e62217 [PubMed: 23614038]
35. Torres-Mendez A, Bonnal S, Marquez Y, Roth J, Iglesias M, Permanyer J, et al.A novel protein domain in an ancestral splicing factor drove the evolution of neural microexons. Nat Ecol Evol2019;3:691–701 [PubMed: 30833759]
36. Nakano Y, Wiechert S, Banfi B. Overlapping Activities of Two Neuronal Splicing Factors Switch the GABA Effect from Excitatory to Inhibitory by Regulating REST. Cell reports2019;27:860–71 e8 [PubMed: 30995482]
37. Lee NS, Evgrafov OV, Souaiaia T, Bonyad A, Herstein J, Lee JY, et al.Non-coding RNAs derived from an alternatively spliced REST transcript (REST-003) regulate breast cancer invasiveness. Scientific reports2015;5:11207 [PubMed: 26053433]
38. Gupta S, Stamatoyannopoulos JA, Bailey TL, Noble WS. Quantifying similarity between motifs. Genome biology2007;8:R24 [PubMed: 17324271]
39. Coleman DJ, Sampson DA, Sehrawat A, Kumaraswamy A, Sun D, Wang Y, et al.Alternative splicing of LSD1+8a in neuroendocrine prostate cancer is mediated by SRRM4. Neoplasia2020;22:253–62 [PubMed: 32403054]
40. Li Y, Xie N, Chen R, Lee AR, Lovnicki J, Morrison EA, et al.RNA Splicing of the BHC80 Gene Contributes to Neuroendocrine Prostate Cancer Progression. European urology2019;76:157–66 [PubMed: 30910347]
41. Chiaverotti T, Couto SS, Donjacour A, Mao JH, Nagase H, Cardiff RD, et al.Dissociation of epithelial and neuroendocrine carcinoma lineages in the transgenic adenocarcinoma of mouse prostate model of prostate cancer. The American journal of pathology2008;172:236–46 [PubMed: 18156212]
42. Rudin CM, Poirier JT, Byers LA, Dive C, Dowlati A, George J, et al.Molecular subtypes of small cell lung cancer: a synthesis of human and mouse model data. Nat Rev Cancer2019;19:289–97 [PubMed: 30926931]
43. Borromeo MD, Savage TK, Kollipara RK, He M, Augustyn A, Osborne JK, et al.ASCL1 and NEUROD1 Reveal Heterogeneity in Pulmonary Neuroendocrine Tumors and Regulate Distinct Genetic Programs. Cell Rep2016;16:1259–72 [PubMed: 27452466]
44. Balanis NG, Sheu KM, Esedebe FN, Patel SJ, Smith BA, Park JW, et al.Pan-cancer Convergence to a Small-Cell Neuroendocrine Phenotype that Shares Susceptibilities with Hematological Malignancies. Cancer cell2019;36:17–34 e7 [PubMed: 31287989]
45. Park JW, Lee JK, Sheu KM, Wang L, Balanis NG, Nguyen K, et al.Reprogramming normal human epithelial tissues to a common, lethal neuroendocrine cancer lineage. Science2018;362:91–5 [PubMed: 30287662]
46. Chen JF, Yang C, Sun Y, Cao D. Expression of novel neuroendocrine marker insulinoma-associated protein 1 (INSM1) in genitourinary high-grade neuroendocrine carcinomas: An immunohistochemical study with specificity analysis and comparison to chromogranin, synaptophysin, and CD56. Pathol Res Pract2020;216:152993
47. Yao JL, Madeb R, Bourne P, Lei J, Yang X, Tickoo S, et al.Small cell carcinoma of the prostate: an immunohistochemical study. The American journal of surgical pathology2006;30:705–12 [PubMed: 16723847]
48. Kreisler A, Strissel PL, Strick R, Neumann SB, Schumacher U, Becker CM. Regulation of the NRSF/REST gene by methylation and CREB affects the cellular phenotype of small-cell lung cancer. Oncogene2010;29:5828–38 [PubMed: 20697351]

49. Shimojo M, Shudo Y, Ikeda M, Kobashi T, Ito S. The small cell lung cancer-specific isoform of RE1-silencing transcription factor (REST) is regulated by neural-specific Ser/Arg repeat-related protein of 100 kDa (nSR100). Mol Cancer Res 2013;11:1258–68 [PubMed: 23928058]
50. Li Y, Donmez N, Sahinalp C, Xie N, Wang Y, Xue H, et al.SRRM4 Drives Neuroendocrine Transdifferentiation of Prostate Adenocarcinoma Under Androgen Receptor Pathway Inhibition. European urology2017;71:68–78 [PubMed: 27180064]
51. Lee AR, Gan Y, Tang Y, Dong X. A novel mechanism of SRRM4 in promoting neuroendocrine prostate cancer development via a pluripotency gene network. EBioMedicine2018;35:167–77 [PubMed: 30100395]
52. Crona J, Backman S, Welin S, Taieb D, Hellman P, Stalberg P, et al.RNA-Sequencing Analysis of Adrenocortical Carcinoma, Pheochromocytoma and Paraganglioma from a Pan-Cancer Perspective. Cancers (Basel)2018;10
53. Ren H, Gao Z, Wu N, Zeng L, Tang X, Chen X, et al.Expression of REST4 in human gliomas in vivo and influence of pioglitazone on REST in vitro. Biochemical and biophysical research communications2015;463:504–9 [PubMed: 26003726]
54. Palm K, Metsis M, Timmusk T. Neuron-specific splicing of zinc finger transcription factor REST/NRSF/XBR is frequent in neuroblastomas and conserved in human, mouse and rat. Brain research Molecular brain research1999;72:30–9 [PubMed: 10521596]
55. Corella AN, Cabiliza Ordonio MVA, Coleman I, Lucas JM, Kaipainen A, Nguyen HM, et al.Identification of Therapeutic Vulnerabilities in Small-cell Neuroendocrine Prostate Cancer. Clinical cancer research : an official journal of the American Association for Cancer Research2020;26:1667–77 [PubMed: 31806643]
56. Tran C, Ouk S, Clegg NJ, Chen Y, Watson PA, Arora V, et al.Development of a second-generation antiandrogen for treatment of advanced prostate cancer. Science2009;324:787–90 [PubMed: 19359544]
57. Li Y, Chan SC, Brand LJ, Hwang TH, Silverstein KA, Dehm SM. Androgen receptor splice variants mediate enzalutamide resistance in castration-resistant prostate cancer cell lines. Cancer Res2013;73:483–9 [PubMed: 23117885]
58. Mollaoglu G, Guthrie MR, Bohm S, Bragelmann J, Can I, Ballieu PM, et al.MYC Drives Progression of Small Cell Lung Cancer to a Variant Neuroendocrine Subtype with Vulnerability to Aurora Kinase Inhibition. Cancer Cell2017;31:270–85 [PubMed: 28089889]
59. Beltran H, Oromendia C, Danila DC, Montgomery B, Hoimes C, Szmulewitz RZ, et al.A Phase II Trial of the Aurora Kinase A Inhibitor Alisertib for Patients with Castration-resistant and Neuroendocrine Prostate Cancer: Efficacy and Biomarkers. Clinical cancer research : an official journal of the American Association for Cancer Research2019;25:43–51 [PubMed: 30232224]

SIGNIFICANCE

This study identifies SRRM3 as a key inducer of cellular plasticity in prostate cancer with neuroendocrine features and delineates distinct neuroendocrine phenotypes to inform therapeutic development and precision medicine applications.

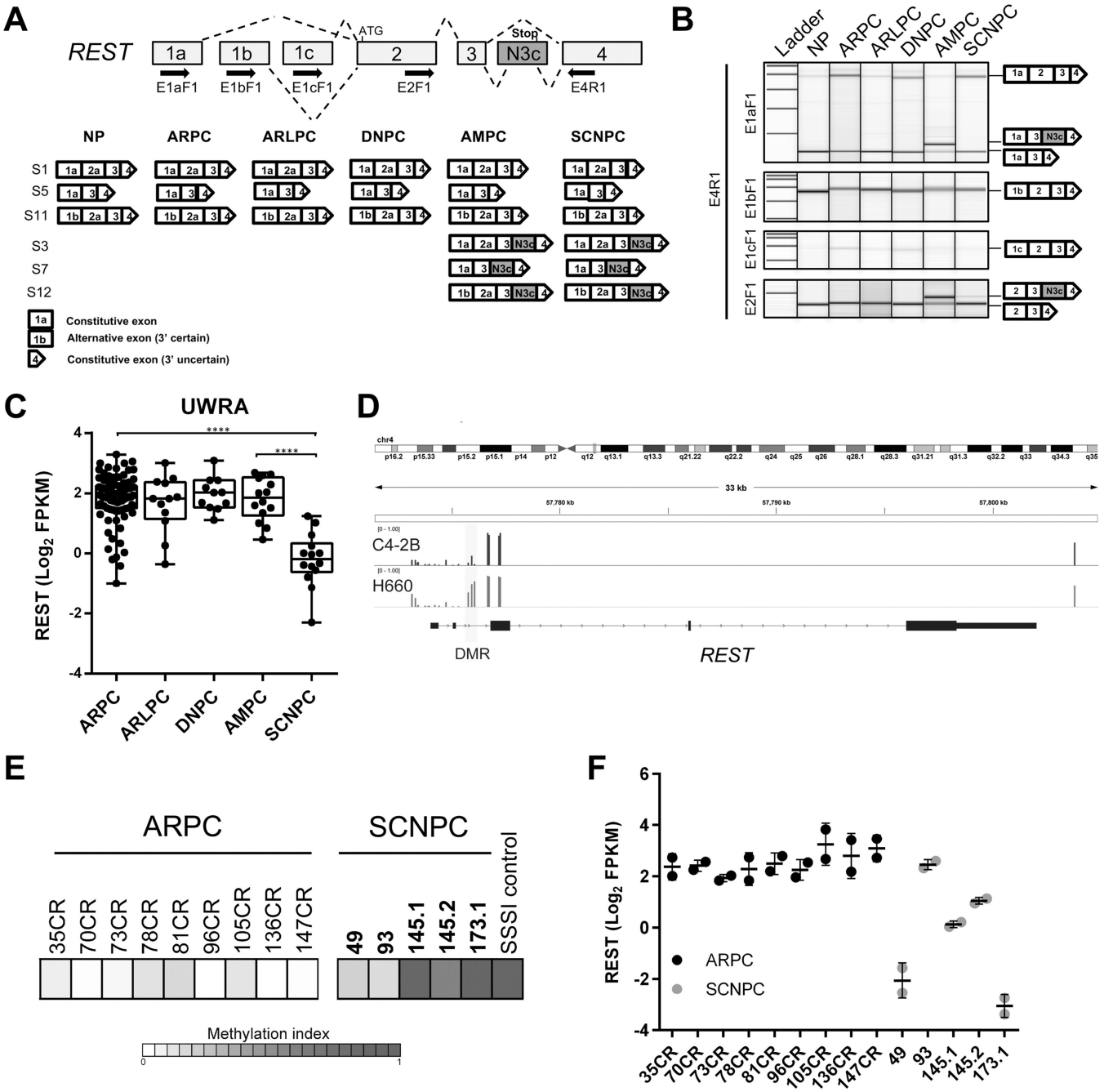

Figure 1. Alternative REST splicing and REST locus hypermethylation occur in NE$^+$ mCRPC.

(**A**) *Top*: *REST* exons with the location of PCR primers (black arrows). *Bottom*: summary of the identified *REST* splice variants in normal prostate (NP; n=5), AR-high prostate cancer (ARPC; n=5), AR-low prostate cancer (ARLPC; n=5), double-negative prostate cancer (DNPC; n=5), amphicrine prostate cancer (AMPC; n=5) and small cell or neuroendocrine prostate cancer (SCNPC; n=4). (**B**) This is a composite image of PCR analyses of representative patient specimens from NP and the 5 mCRPC phenotypes using forward primers specific to *REST* exon 1a (E1aF1), exon 1b (E1bF1), exon 1c (E1cF1) and exon 2 (E2F1). All forward primers were paired with a reverse primer specific to *REST* exon 4

(E4R1). (**C**) Boxplot of *REST* mRNA expression from the UWRA mCRPC cohort (ARPC; n=88, AMPC; n=14, ARLPC; n=11, DNPC; n=10, SCNPC; n=14). (**D**) Methylation analysis of the *REST* locus in C4–2B and NCI-H660 cells using EPIC arrays. DMR = differentially methylated region. (**E**) COMPARE-MS heatmap of *REST* methylation in LuCaP PDX models. Results are expressed as ct-values of the samples of interest normalized to ct-values of the SSSI control (*in vitro* fully methylated male genomic DNA) and are colored according to scale. (**F**) Plot of *REST* expression in LuCaP PDX models (n=2 for each model). Black = ARPC models, grey = SCNPC models. ****P-value < 0.0001; One-way ANOVA with Tukey's multiple comparisons test.

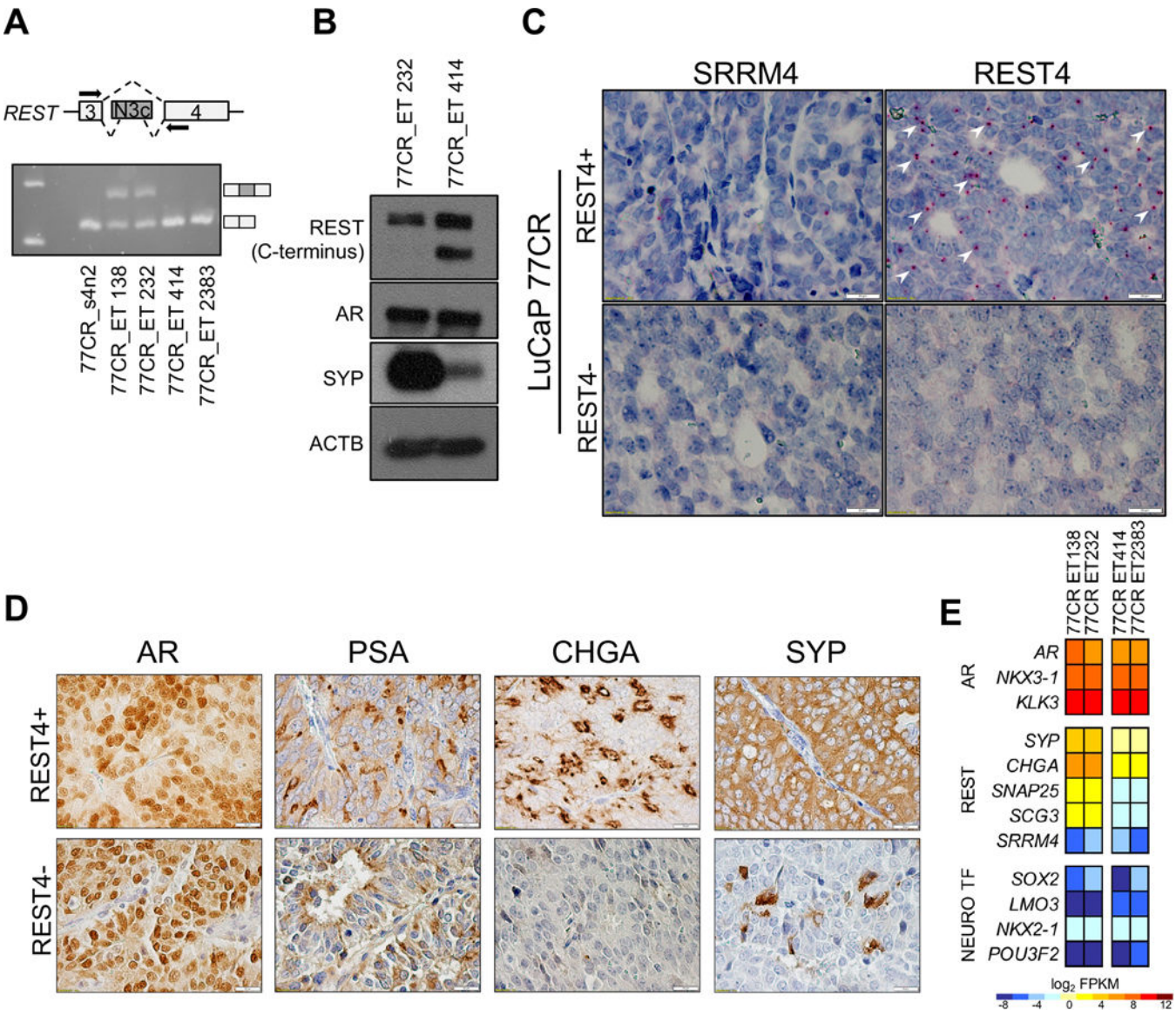

Figure 2. REST alternative splicing occurs without SRRM4 expression in the AMPC LuCaP 77CR PDX model.

(**A**) PCR analysis of LuCaP 77CR tumor specimens (n=5) using primers specific to *REST* that span exon N3c. (**B**) Immunoblot of whole tumor extracts from 77CR tumor specimens. ACTB was used as a loading control. (**C**) BaseScope analyses of LuCaP 77CR tumor sections using probes specific to SRRM4 and REST exon N3c (REST4). White arrows point to examples of positive chromogenic FastRED readouts. (**D**) Immunohistochemistry of LuCaP 77CR tumors represented in (C). Bars = 20 microns. (**E**) RNAseq heatmap of LuCaP 77CR specimens depicting AR (top), REST repressed genes (middle) and transcription factors associated with SCNPC (bottom). Results are expressed as $\log_2$ FPKM and are colored according to scale.

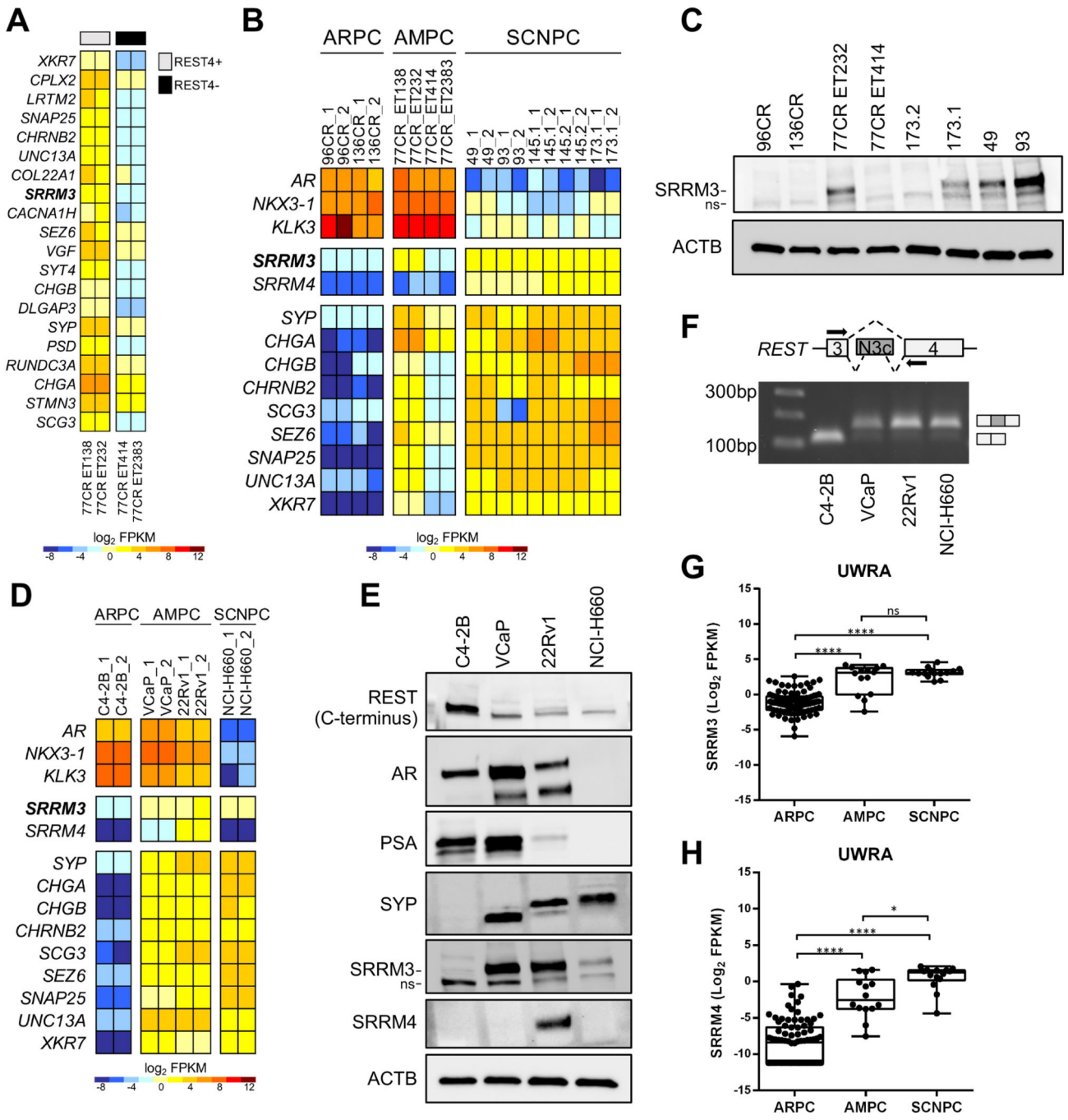

Figure 3. SRRM3 is expressed in PDX models, CRPC cell lines and patient tumors with NE differentiation and associates with attenuated REST activity.

(**A**) RNAseq heatmap of top differentially expressed genes in LuCaP 77CR tumors +/− REST4 expression. (**B**) RNAseq heatmap of LuCaP PDX models. Bottom panel of genes are SRRM3/REST-associated genes. (**C**) Immunoblot of whole tumor extracts from LuCaP PDX models. ACTB was used as a loading control; ns = non-specific band. (**D**) RNAseq heatmap of CRPC cell lines. All heatmaps are shown as $\log_2$ FPKM and are colored according to scale. (**E**) Immunoblots of whole cell extracts from C4–2B, VCaP, 22Rv1 and NCI-H660

cells. Blots were probed with indicated antibodies and ACTB was the loading control; ns = non-specific band. (**F**) PCR analysis of CRPC cell lines using primers specific to *REST*. Boxplots of (**G**) *SRRM3* and (**H**) *SRRM4* expression in ARPC (n=88), AMPC (n=14) and SCNPC (n=14) mCRPC specimens from UWRA RNAseq. Each point represents a single tumor. *p<0.05, ****p< 0.0001, ns = not significant; One-way ANOVA with Tukey's multiple comparisons test.

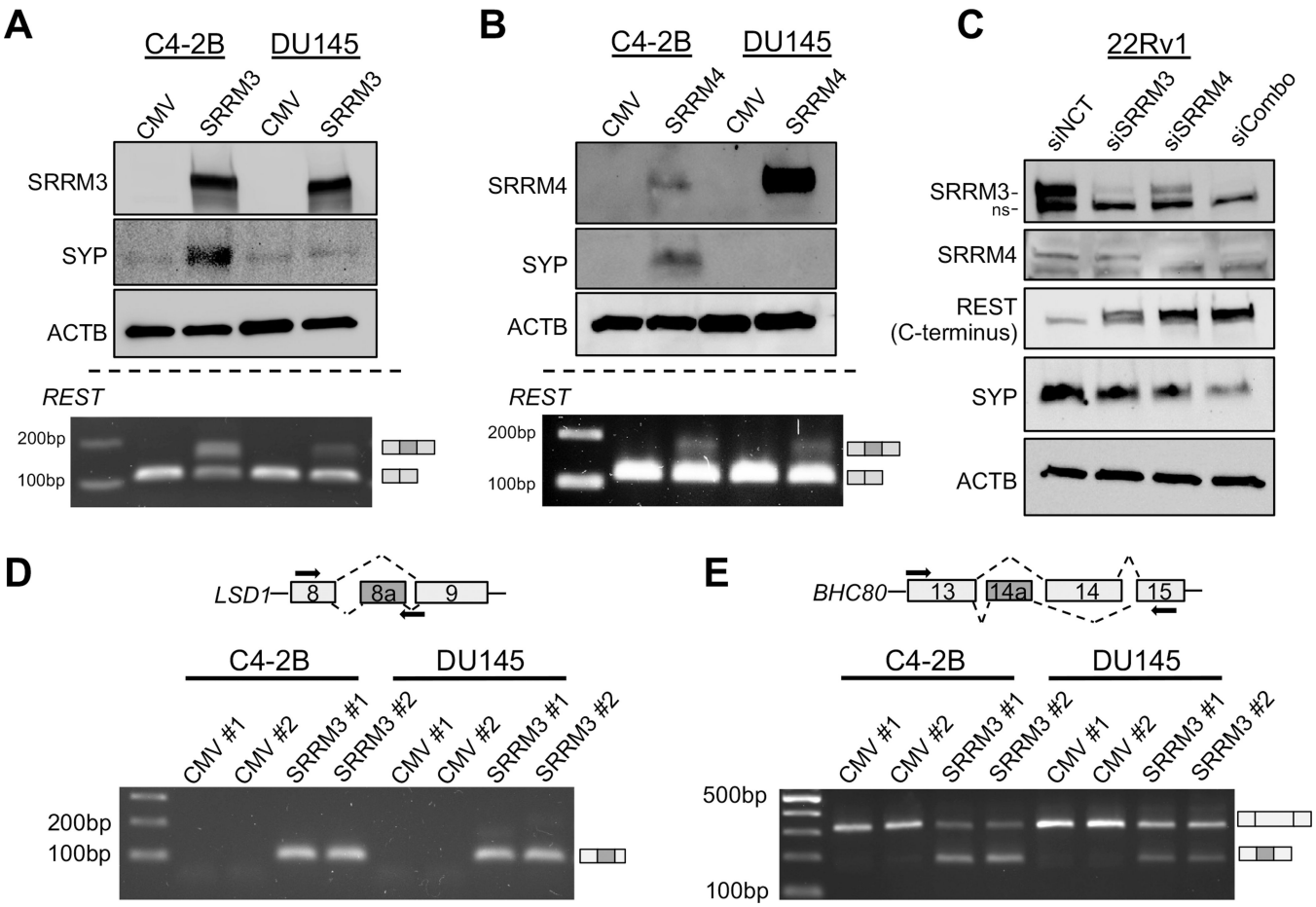

Figure 4. SRRM3 and SRRM4 induce REST alternative splicing to attenuate REST activity and alternatively splice the same transcripts.

C4-2B and DU145 cells transfected with either (**A**) SRRM3, (**B**) SRRM4 expression vectors or CMV negative control vectors. Top panels (above dotted lines) are representative immunoblots using indicated antibodies and bottom panels (below dotted lines) are PCR analyses using primers specific to *REST* exon N3c alternative splicing. (**C**) Immunoblots of 22Rv1 cells transfected with siRNAs to SRRM3, SRRM4, SRRM3 and SRRM4 (siCombo) or non-targeting siRNA (siNCT). Blots were probed with primary antibodies as indicated; ns = non-specific band. PCR analysis of (**D**) *LSD1* and (**E**) *BHC80* alternative splicing in C4–2B or DU145 cells transfected with SRRM3 expression vector or CMV control. Results show amplicons from biological duplicates and the location of primers are depicted as black arrows.

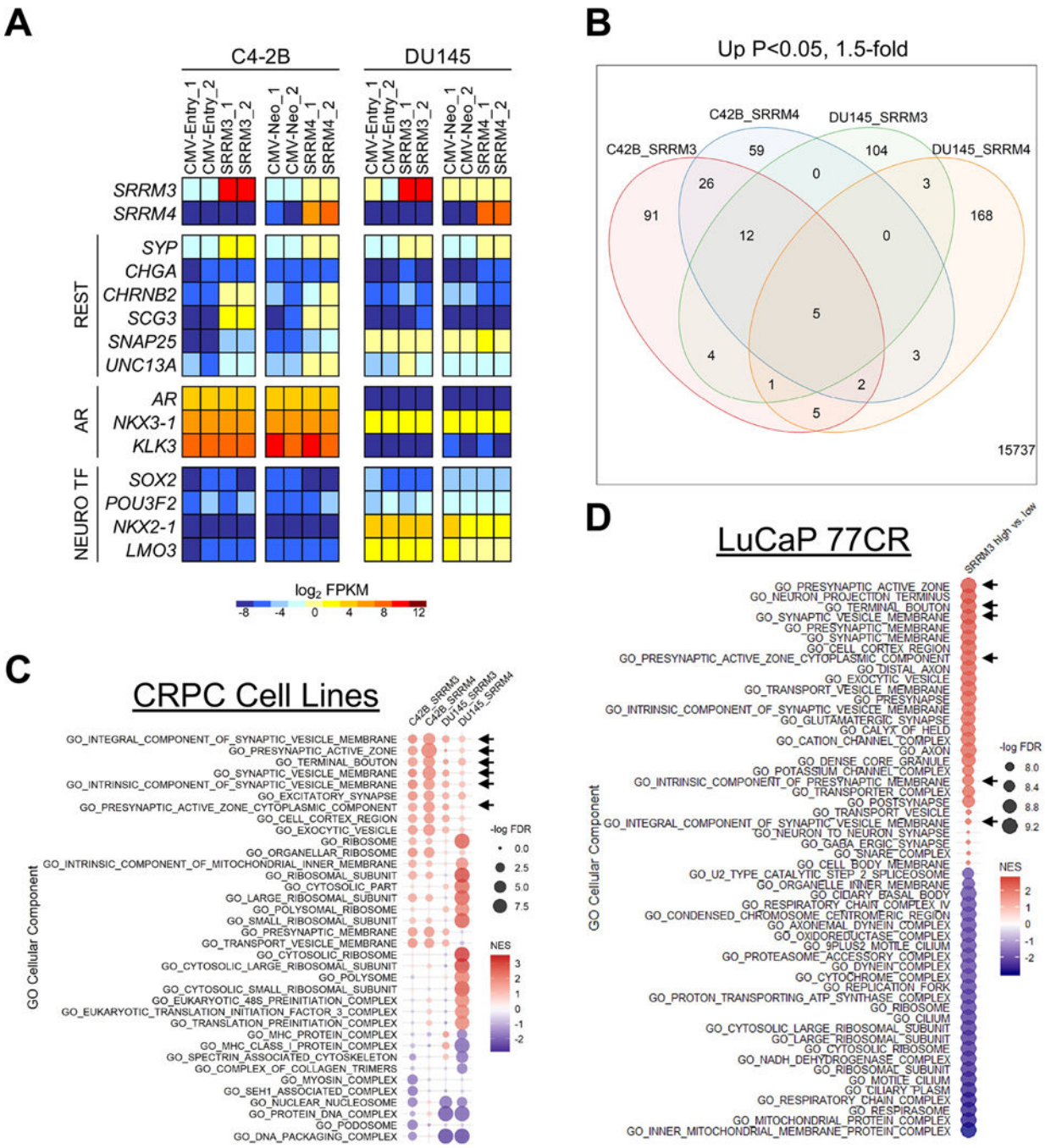

Figure 5. Ectopic expression of SRRM3 or SRRM4 significantly alters REST-regulated gene expression and promotes NE cellular plasticity in C4–2B and DU145 cells.

(**A**) RNAseq heatmap of C4–2B and DU145 cells transfected with either SRRM3, SRRM4 or CMV expression vectors. Results are shown as $\log_2$ FPKM and are colored according to scale. (**B**) Venn diagram showing the overlap of significantly upregulated genes (FC>1.5, p<0.05) between C4–2B and DU145 cells expressing SRRM3 or SRRM4 vectors compared to CMV control. GO Cellular Component summary plots of differentially expressed genes in (**C**) CRPC cells from A and (**D**) LuCaP 77CR PDX tumors with high or low SRRM3

expression. Pathways with FDR<0.05 in at least one group are shown and arrows point to overlapping NE pathways.

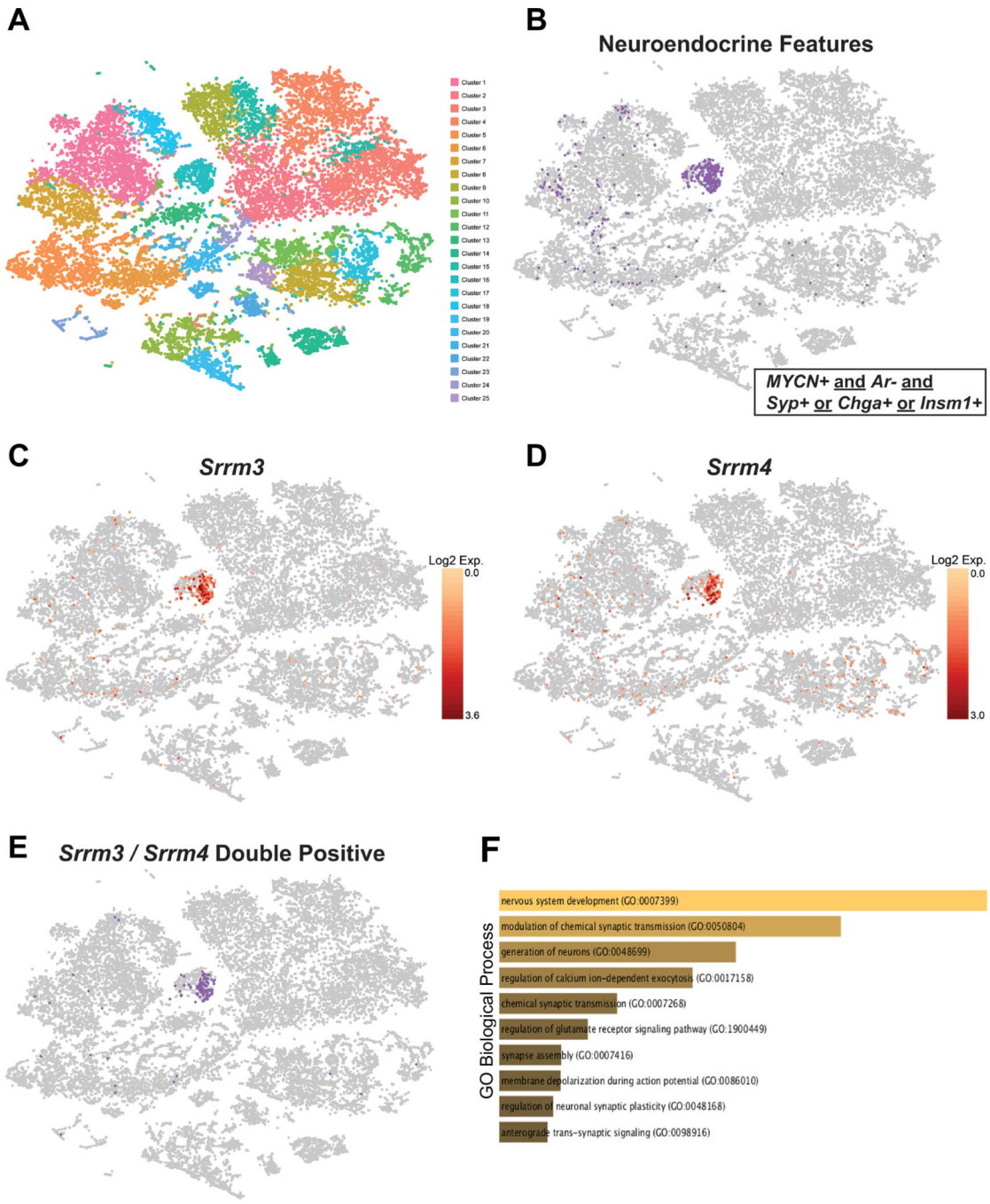

Figure 6. *Srrm3* and *Srrm4* are expressed in SCNPC-like tumor cells from a MYCN-driven CRPC GEMM model.

(**A**) t-SNE plot and clustering of combined single cell RNAseq data from 8-week-old *Pb-Cre+; Pten*$^{f/f}$*; MYCN+; Rb1*$^{f/f}$ prostate tumors (n=3). Data comprised of 22,461 cells. (**B**) Identification of SCNPC-like cells that are *MYCN+* and *Ar-* as well as positive for at least one NE marker (*Syp+*, *Chga+*, *Insm1+*). Expression levels of (**C**) *Srrm3* and (**D**) *Srrm4* in scRNAseq data. Data is represented as $\log_2$ expression of the normalized read lengths and are colored according to scale. (**E**) Identification of cells that are *Srrm3* and *Srrm4*

double positive. (**F**) Enrichr gene ontology analysis of the significant differentially expressed genes ($p<0.05$) in SCNPC-like cells that are *Srrm3*+ or *Srrm4*+ compared to ARPC-like cells (*Ar*+/*Syp*-). Results are ranked according to P-value.

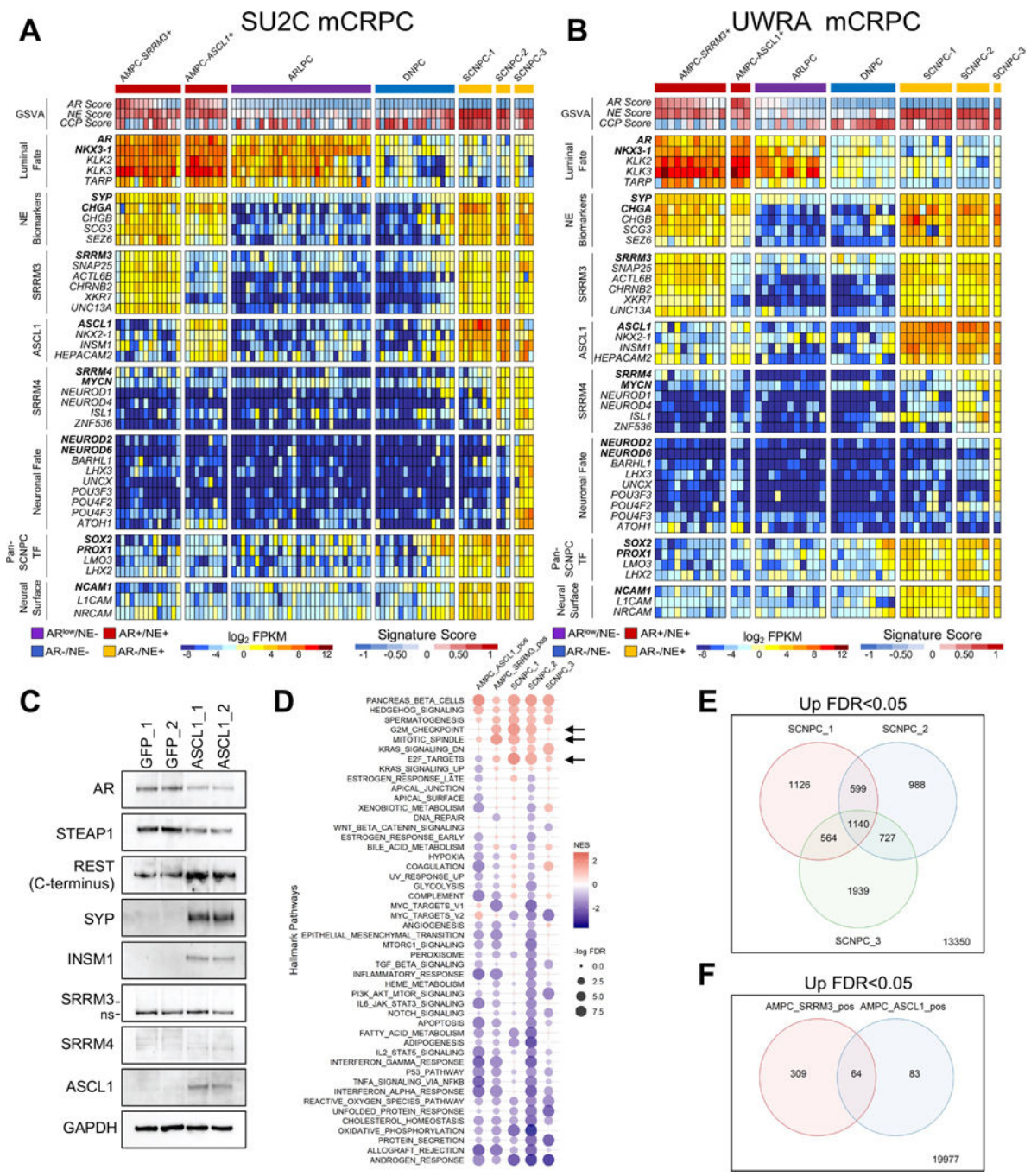

Figure 7. SRRM3 and SRRM4 identify molecular subtypes of NE$^+$ mCRPC.

RNAseq heatmaps of CRPC metastases from (**A**) Stand Up to Cancer (SU2C; n=84) and (**B**) University of Washington Rapid Autopsy (UWRA; n=49) segregated according to differential expression of transcription factors and NE biomarkers from literature. Results are expressed as $\log_2$ FPKM (expression) or as GSVA (activity scores) and are colored according to scale. Amphicrine = red, AR-low = purple, double-negative = blue, small cell or neuroendocrine = gold. (**C**) Immunoblot of C4–2B cells transduced with constructs encoding ASCL1 or GFP (control). GAPDH was used as a loading control and blots show

lysates from two independent experiments; ns = non-specific band. (**D**) GSEA summary of the Hallmark Pathways in AMPC-*SRRM3*$^{+}$, AMPC-*ASCL1*$^{+}$, SCNPC-1, SCNPC-2 and SCNPC-3 compared to ARPC in the SU2C mCRPC dataset. Pathways with FDR<0.05 in at least one group are shown. Venn diagrams of (**E**) SCNPC and (**F**) AMPC molecular phenotypes depicting unique and overlapping upregulated genes (FDR<0.05) relative to ARPC.